


Efficiently evaluating the Krieger-Li-Iafrate and common-energy-denominator approximations in the frequency-dependent Sternheimer scheme

Fabian Hofmann, Ingo Schelter, and Stephan Kümmel
Theoretical Physics IV, University of Bayreuth, 95440 Bayreuth, Germany

 (Received 25 November 2018; revised manuscript received 18 January 2019; published 20 February 2019)

We show that within the Krieger-Li-Iafrate and common-energy-denominator approximations, the linearized time-dependent Kohn-Sham equations for orbital functionals can be solved very efficiently using the frequency-dependent Sternheimer scheme. The Kohn-Sham response can be obtained without the need to explicitly evaluate the exchange-correlation kernel as a functional derivative with respect to the density. Instead, it suffices to compute functional derivatives with respect to the orbitals. The scheme allows for the computationally efficient use of orbital functional potential approximations in Kohn-Sham response theory.

DOI: [10.1103/PhysRevA.99.022507](https://doi.org/10.1103/PhysRevA.99.022507)

I. INTRODUCTION: TIME-DEPENDENT DENSITY-FUNCTIONAL THEORY AND ORBITAL FUNCTIONALS

Time-dependent density-functional theory (TDDFT) has become one of the most often used approaches to compute optical properties of molecules and nanostructures. The accuracy of TDDFT has greatly increased with the advent of functionals that depend explicitly on the orbitals and are thus implicit density functionals [1,2]. Global hybrid functionals [3–5], local hybrids [6–10], and range-separated hybrids [11–17] exploit the combination of orbital-dependent exact exchange (EXX) with semilocal density functionals in order to achieve a remarkable accuracy. Time-dependent self-interaction corrections (SICs) in different variants [18–21] use the orbital dependence in order to correct for the spurious Hartree self-interaction and are particularly interesting for the description of electron emission [22–26] and charge-transfer processes [27–29].

So far, orbital functionals are mostly used in TDDFT in the generalized Kohn-Sham scheme, with individual potentials for each orbital. First introduced pragmatically as an adiabatic extension of the ground-state generalized Kohn-Sham scheme, the time-dependent (TD) generalized Kohn-Sham approach can also be formally justified [30]. The generalized Kohn-Sham scheme has become the de facto standard for the use of orbital functionals in TDDFT.

Despite the unquestionable successes of the TD generalized Kohn-Sham approach, it would be desirable to be able to use orbital functionals also in TD Kohn-Sham theory, i.e., with equations that use the same global multiplicative potential for all orbitals. From a computational point of view, the use of a single local potential is attractive because it parallelizes nicely and can be used efficiently with many different types of numerical realizations, including numerical grids. From a conceptual point of view, the Kohn-Sham approach is attractive because the Kohn-Sham system is uniquely defined. Furthermore, as the Kohn-Sham potential is the same for occupied and unoccupied orbitals, the unoccupied Kohn-Sham eigenvalue spectrum has attractive features

that are typically not shared by the corresponding generalized Kohn-Sham spectrum, such as a Rydberg series resulting from Fock exchange [1,31]. Also, for the purposes of functional development, the concepts of Kohn-Sham theory serve as an important guideline for learning how to incorporate spatial and temporal nonlocalities [32–34].

The use of orbital functionals in TD Kohn-Sham theory has so far been limited by the difficulties that are associated with solving the TD optimized effective potential (TDOEP) equation [35]. In the linear-response regime, evaluating the exchange-correlation (xc) kernel $f_{xc}(\mathbf{r}, t, \mathbf{r}', t')$ as a second functional derivative of the xc action functional with respect to the density leads to involved mathematical expressions. The evaluation of the xc kernel for orbital functionals and its numerical realization have been carried out in several important works [36–46]. However, the resulting expressions are challenging to code, not always easy to interpret, and in some of the works the adiabatic approximation has been invoked [36–38]. In the real-time propagation approach to TDDFT [47], one need not evaluate $f_{xc}(\mathbf{r}, t, \mathbf{r}', t')$, as only the potential $v_{xc}(\mathbf{r}, t)$ is required. However, solving the TDOEP equation in the real-time propagation context proved very challenging. Straightforward propagation is fraught with computational difficulties [48–50], and progress made [51] has so far been restricted to one-dimensional model systems. A particularly sobering aspect of the combination of real-time techniques and orbital functionals is the finding that approximations to the OEP such as the Krieger-Li-Iafrate (KLI) approximation [52] and the common-energy-denominator approximation (CEDA) [53] (also termed the localized Hartree-Fock approximation [54]) cannot generally be used. Although these approximations often work quite reliably in ground-state calculations, they, as well as related approximations, frequently become unstable in real-time propagations [29,55,56]. As a consequence, there are only a few systems for which reliable TD Kohn-Sham results using orbital functionals are available.

In this paper we show how approximate Kohn-Sham potentials for orbital functionals such as the KLI approximation and CEDA can be used in TD Kohn-Sham theory without

suffering from instabilities and in a numerically efficient way. The decisive idea is to use the frequency-dependent Sternheimer scheme [57,58]. In this way, one can avoid the explicit evaluation of f_{xc} for orbital functionals, as well as the accumulation of numerical inaccuracies that hinders real-time propagation with the KLI and CEDA potentials. The power of the Sternheimer approach, which has been brought to bear previously in different areas of electronic structure theory [59–65], can thus be harnessed for TDDFT.

In the following, we first discuss the linearization of orbital-dependent quantities in Kohn-Sham theory in general and then use this concept to set up Sternheimer equations for the linear response following from the KLI and CEDA potentials. After a brief recapitulation of the frequency-dependent Sternheimer scheme, we demonstrate the reliability and accuracy of our method for several paradigm test cases as a proof of concept. We conclude with a summary and an outlook on future work.

II. LINEARIZATION OF ORBITAL-DEPENDENT QUANTITIES IN THE KOHN-SHAM FRAMEWORK

In TDDFT, the usual way of calculating the linear response of a (spin-)density-dependent quantity \mathcal{O} to an external perturbation is by means of an expansion with respect to the linear spin-density response $n_\sigma^{(1)}(\mathbf{r}, t)$ that results from the perturbation [66]:

$$\mathcal{O}^{(1)} = \sum_{\tau=\uparrow,\downarrow} \int dt' \int d^3r' \left[\frac{\delta \mathcal{O}}{\delta n_\tau(\mathbf{r}', t')} \right]^{(0)} n_\tau^{(1)}(\mathbf{r}', t'). \quad (1)$$

The superscript (0) indicates that the term in square brackets is evaluated in the unperturbed system, σ and τ are spin indices, \mathbf{r} and \mathbf{r}' are spatial coordinates, and t and t' are time variables. Applying Eq. (1) to the exchange-correlation potential $v_{xc\sigma}(\mathbf{r}, t)$ introduces the xc kernel $f_{xc\sigma\tau}$ [66,67]:

$$f_{xc\sigma\tau}(\mathbf{r}, \mathbf{r}', t, t') = \left[\frac{\delta v_{xc\sigma}(\mathbf{r}, t)}{\delta n_\tau(\mathbf{r}', t')} \right]^{(0)}. \quad (2)$$

In this work, we are dealing with quantities [such as approximations to $v_{xc\sigma}(\mathbf{r}, t)$] that are known as functionals of the time-dependent occupied orbitals of the Kohn-Sham system. Consider any occupied-orbital-dependent quantity

$$\mathcal{O} = \mathcal{O} \left[\left\{ \varphi_{k\alpha}, \varphi_{k\alpha}^* \right\}_{\substack{\alpha=\uparrow,\downarrow \\ k=1,\dots,N_\alpha}} \right] \quad (3)$$

[it can be complex and depend on further variables, e.g., $\mathcal{O}_\sigma(\mathbf{r}, t) \in \mathbb{C}$]. In the time-dependent Kohn-Sham framework, the orbitals are determined by the density and the initial state [66–68]. For the perturbation theory setting where propagations start in the ground state (GS), the Kohn-Sham orbitals are unique functionals of the density,

$$\varphi_{i\sigma}(\mathbf{r}, t) = \varphi_{i\sigma}[n_\uparrow, n_\downarrow](\mathbf{r}, t). \quad (4)$$

As a consequence, \mathcal{O} itself is also a functional of the density,

$$\mathcal{O}[\{n_\beta\}] = \mathcal{O}[\{\varphi_{k\alpha}[\{n_\beta\}], \varphi_{k\alpha}^*[\{n_\beta\}]\}]. \quad (5)$$

This means that \mathcal{O} can be linearized in the perturbation using Eq. (1). However, as it depends on the density via the occupied

orbitals, the functional derivatives in Eqs. (1) and (2) have to be calculated with the help of the chain rule,

$$\begin{aligned} \frac{\delta \mathcal{O}}{\delta n_\tau(\mathbf{r}', t')} &= \sum_{\gamma=\uparrow,\downarrow} \sum_{j=1}^{N_\gamma} \int dt'' \int d^3r'' \\ &\times \left\{ \frac{\delta \mathcal{O}}{\delta \varphi_{j\gamma}(\mathbf{r}'', t'')} \frac{\delta \varphi_{j\gamma}(\mathbf{r}'', t'')}{\delta n_\tau(\mathbf{r}', t')} \right. \\ &\left. + \frac{\delta \mathcal{O}}{\delta \varphi_{j\gamma}^*(\mathbf{r}'', t'')} \frac{\delta \varphi_{j\gamma}^*(\mathbf{r}'', t'')}{\delta n_\tau(\mathbf{r}', t')} \right\}. \quad (6) \end{aligned}$$

The derivatives $\delta \varphi_{j\gamma}(\mathbf{r}'', t'')/\delta n_\tau(\mathbf{r}', t')$ are not known analytically and have to be calculated from complicated integral equations. This step so far has been a major hurdle in the use of orbital-dependent functionals. A central piece of our work here is to show how the explicit evaluation of these derivatives can be avoided: First, we express the linear response of the TD Kohn-Sham orbitals to an external perturbation in two different ways, namely, as a solution of the Sternheimer equations on the one hand and as a formal density expansion as in Eq. (1) on the other. We can then use the latter to rewrite the chain rule expression for $\mathcal{O}^{(1)}$ in terms of the response of the orbitals, which we calculate using the former. This procedure is explained in detail in the following.

In the first step, we recall the Sternheimer scheme in the form that we recently discussed in detail in Ref. [58]. We consider perturbations of the form

$$v_{\text{ext},\sigma}(\mathbf{r}, t) = [v_{\text{ext},\sigma}^{(+)}(\mathbf{r})e^{-i\omega t} + \text{c.c.}]e^{\eta t}, \quad \omega, \eta > 0, \quad (7)$$

i.e., the perturbations are exponentially switched on harmonic oscillations. Here $v_{\text{ext},\sigma}^{(+)}(\mathbf{r})$ denotes the Fourier component and specifies the spatial and spin dependence of the perturbation. The specific forms that we used in the calculations presented in this work are given in Eqs. (54) and (62). For a general discussion of the possible spin and spatial dependences of the perturbation, we refer to Ref. [58].

As shown in Ref. [58], the zeroth- and first-order contributions to the perturbation series of the TD Kohn-Sham orbitals can be written as

$$\varphi_{j\sigma}^{(0)}(\mathbf{r}, t) = \phi_{j\sigma}(\mathbf{r})e^{-i(\varepsilon_{j\sigma}/\hbar)t} \quad (8)$$

and

$$\begin{aligned} \varphi_{j\sigma}^{(1)}(\mathbf{r}, t) &= e^{-i(\varepsilon_{j\sigma}/\hbar)t} \{ [\varphi_{j\sigma}^{(+)}(\mathbf{r})e^{-i\omega t} + \varphi_{j\sigma}^{(-)*}(\mathbf{r})e^{i\omega t}] e^{\eta t} \\ &- i\phi_{j\sigma}(\mathbf{r})\varepsilon_{j\sigma}^{(1)}(t) \}, \quad (9) \end{aligned}$$

where $\phi_{j\sigma}(\mathbf{r})$ and $\varepsilon_{j\sigma}$ are GS orbitals and eigenvalues of the unperturbed Kohn-Sham system, the orbitals $\phi_{j\sigma}$ are chosen to be real, and

$$\varepsilon_{j\sigma}^{(1)}(t) = [\varepsilon_{j\sigma}^{(+)}e^{-i\omega t} + \text{c.c.}]e^{\eta t} \quad (10)$$

is real as well. The quantities $\varphi_{j\sigma}^{(\pm)}(\mathbf{r})$ are Fourier components of the first-order response of the orbitals and will be determined by the Sternheimer equations [see Eq. (16) below].

The linear response of the density and of the Hartree-exchange-correlation potential then takes the form

$$n_\sigma^{(1)}(\mathbf{r}, t) = [n_\sigma^{(+)}(\mathbf{r})e^{-i\omega t} + \text{c.c.}]e^{\eta t}, \quad (11)$$

$$n_{\sigma}^{(+)}(\mathbf{r}) = \sum_{i=1}^{N_{\sigma}} \phi_{i\sigma}(\mathbf{r}) [\varphi_{i\sigma}^{(+)}(\mathbf{r}) + \varphi_{i\sigma}^{(-)}(\mathbf{r})], \quad (12)$$

and

$$v_{\text{Hxc},\sigma}^{(1)}(\mathbf{r}, t) = [v_{\text{Hxc},\sigma}^{(+)}(\mathbf{r})e^{-i\omega t} + \text{c.c.}]e^{i\eta t}, \quad (13)$$

where the latter is derived from Eqs. (1) and (11). The Hartree contribution to $v_{\text{Hxc},\sigma}^{(+)}$ can be calculated from Poisson's equation

$$\nabla^2 v_{\text{H}}^{(+)}(\mathbf{r}) = -4e^2\pi [n_{\uparrow}^{(+)}(\mathbf{r}) + n_{\downarrow}^{(+)}(\mathbf{r})], \quad (14)$$

where e is the elementary charge. While the energy response components $\varepsilon_{j\sigma}^{(+)}$ mentioned above eventually drop out of our equations (cf. Sec. III) and thus never need to be computed, they could in principle be calculated from [58]

$$\varepsilon_{j\sigma}^{(+)} = i \int d^3r \frac{\phi_{j\sigma}^2(\mathbf{r}) [v_{\text{ext},\sigma}^{(+)}(\mathbf{r}) + v_{\text{Hxc},\sigma}^{(+)}(\mathbf{r})]}{\hbar(\omega + i\eta)}. \quad (15)$$

Finally, the Sternheimer equations determining the orbital response components $\varphi_{j\sigma}^{(\pm)}$ read

$$\begin{aligned} & [\hat{h}_{\sigma} - \varepsilon_{j\sigma} \mp \hbar(\omega + i\eta)] \varphi_{j\sigma}^{(\pm)}(\mathbf{r}) \\ &= -\hat{Q}_{j\sigma} [v_{\text{ext},\sigma}^{(+)}(\mathbf{r}) + v_{\text{Hxc},\sigma}^{(+)}(\mathbf{r})] \phi_{j\sigma}(\mathbf{r}), \end{aligned} \quad (16)$$

with the additional condition

$$\langle \phi_{j\sigma} | \varphi_{j\sigma}^{(\pm)} \rangle = \int d^3r \phi_{j\sigma}(\mathbf{r}) \varphi_{j\sigma}^{(\pm)}(\mathbf{r}) = 0. \quad (17)$$

Here

$$\hat{Q}_{j\sigma} := 1 - |\phi_{j\sigma}\rangle\langle\phi_{j\sigma}| \quad (18)$$

projects onto the subspace orthogonal to $\phi_{j\sigma}$ and \hat{h}_{σ} is the unperturbed (GS) Kohn-Sham Hamiltonian. To perform a linear-response calculation in the Sternheimer scheme, we thus need an expression for $v_{\text{xc}\sigma}^{(+)}(\mathbf{r})$ in terms of the linear response of the spin density or of the orbitals, so that Eq. (16) can be solved self-consistently.

In the second step we note that due to the orbitals' density dependence (4), an alternative expression for their first-order response can be derived by applying Eq. (1) to them. This leads to

$$v_{j\sigma}^{(1)}(\mathbf{r}, t) = \sum_{\tau=\uparrow,\downarrow} \int dt' \int d^3r' \left[\frac{\delta\varphi_{j\sigma}(\mathbf{r}, t)}{\delta n_{\tau}(\mathbf{r}', t')} \right]^{(0)} n_{\tau}^{(1)}(\mathbf{r}', t'), \quad (19)$$

as well as a similar relation for the response of the complex conjugate orbitals, $\varphi_{j\sigma}^{*(1)}(\mathbf{r}, t) = [\varphi_{j\sigma}^{(1)}(\mathbf{r}, t)]^*$. We can use this to rewrite $\mathcal{O}^{(1)}$ after applying the chain rule (6) in Eq. (1):

$$\begin{aligned} \mathcal{O}^{(1)} &= \sum_{\tau=\uparrow,\downarrow} \int dt' \int d^3r' \sum_{\gamma=\uparrow,\downarrow} \sum_{j=1}^{N_{\gamma}} \int dt'' \int d^3r'' \left\{ \left[\frac{\delta\mathcal{O}}{\delta\varphi_{j\gamma}(\mathbf{r}'', t'')} \right]^{(0)} \left[\frac{\delta\varphi_{j\gamma}(\mathbf{r}'', t'')}{\delta n_{\tau}(\mathbf{r}', t')} \right]^{(0)} \right. \\ &\quad \left. + \left[\frac{\delta\mathcal{O}}{\delta\varphi_{j\gamma}^*(\mathbf{r}'', t'')} \right]^{(0)} \left[\frac{\delta\varphi_{j\gamma}^*(\mathbf{r}'', t'')}{\delta n_{\tau}(\mathbf{r}', t')} \right]^{(0)} \right\} n_{\tau}^{(1)}(\mathbf{r}', t') \\ &= \sum_{\gamma=\uparrow,\downarrow} \sum_{j=1}^{N_{\gamma}} \int dt'' \int d^3r'' \left\{ \left[\frac{\delta\mathcal{O}}{\delta\varphi_{j\gamma}(\mathbf{r}'', t'')} \right]^{(0)} \sum_{\tau=\uparrow,\downarrow} \int dt' \int d^3r' \left[\frac{\delta\varphi_{j\gamma}(\mathbf{r}'', t'')}{\delta n_{\tau}(\mathbf{r}', t')} \right]^{(0)} n_{\tau}^{(1)}(\mathbf{r}', t') \right. \\ &\quad \left. + \left[\frac{\delta\mathcal{O}}{\delta\varphi_{j\gamma}^*(\mathbf{r}'', t'')} \right]^{(0)} \sum_{\tau=\uparrow,\downarrow} \int dt' \int d^3r' \left[\frac{\delta\varphi_{j\gamma}^*(\mathbf{r}'', t'')}{\delta n_{\tau}(\mathbf{r}', t')} \right]^{(0)} n_{\tau}^{(1)}(\mathbf{r}', t') \right\} \\ &\stackrel{(19)}{=} \sum_{\gamma=\uparrow,\downarrow} \sum_{j=1}^{N_{\gamma}} \int dt'' \int d^3r'' \left\{ \left[\frac{\delta\mathcal{O}}{\delta\varphi_{j\gamma}(\mathbf{r}'', t'')} \right]^{(0)} \varphi_{j\gamma}^{(1)}(\mathbf{r}'', t'') + \left[\frac{\delta\mathcal{O}}{\delta\varphi_{j\gamma}^*(\mathbf{r}'', t'')} \right]^{(0)} \varphi_{j\gamma}^{(1)*}(\mathbf{r}'', t'') \right\}. \end{aligned}$$

After renaming the summation indices and integration variables, we arrive at

$$\begin{aligned} \mathcal{O}^{(1)} &= \sum_{\tau=\uparrow,\downarrow} \int dt' \int d^3r' \left[\frac{\delta\mathcal{O}}{\delta n_{\tau}(\mathbf{r}', t')} \right]^{(0)} n_{\tau}^{(1)}(\mathbf{r}', t') \\ &= \sum_{\tau=\uparrow,\downarrow} \sum_{j=1}^{N_{\tau}} \int dt' \int d^3r' \left\{ \left[\frac{\delta\mathcal{O}}{\delta\varphi_{j\tau}(\mathbf{r}', t')} \right]^{(0)} \varphi_{j\tau}^{(1)}(\mathbf{r}', t') + \left[\frac{\delta\mathcal{O}}{\delta\varphi_{j\tau}^*(\mathbf{r}', t')} \right]^{(0)} \varphi_{j\tau}^{(1)*}(\mathbf{r}', t') \right\}. \end{aligned} \quad (20)$$

We have thus arrived at an important insight: The expansion with respect to the density response is equivalent to an expansion with respect to the linear response of the Kohn-Sham orbitals.

A special case of particular interest results when we apply Eq. (20) to an orbital-dependent expression for the xc potential,

$$v_{\text{xc}\sigma}^{(1)}(\mathbf{r}, t) = \sum_{\tau=\uparrow,\downarrow} \sum_{j=1}^{N_{\tau}} \int dt' \int d^3r' \left\{ \left[\frac{\delta v_{\text{xc}\sigma}(\mathbf{r}, t)}{\delta\varphi_{j\tau}(\mathbf{r}', t')} \right]^{(0)} \varphi_{j\tau}^{(1)}(\mathbf{r}', t') + \left[\frac{\delta v_{\text{xc}\sigma}(\mathbf{r}, t)}{\delta\varphi_{j\tau}^*(\mathbf{r}', t')} \right]^{(0)} \varphi_{j\tau}^{(1)*}(\mathbf{r}', t') \right\}. \quad (21)$$

This shows that one can calculate the linear xc potential response using an orbital expansion instead of a density expansion. Although this expression is still strictly within the Kohn-Sham scheme, the computational effort has basically been reduced to calculating functional derivatives with respect to the orbitals as in the generalized Kohn-Sham scheme.

Note that even an orbital-adiabatic potential, i.e., one that at time t only depends on the orbitals at time t , is a nonadiabatic, nonlocal density functional. When the potential is linearized using Eq. (21), the corresponding memory is implicitly contained in the response of the orbitals: If we were to write the response of the potential in terms of a kernel, we would have to reinsert Eq. (19). This would introduce the space and time nonlocality to the kernel in form of the derivatives $\delta\varphi_{j\sigma}(\mathbf{r}, t)/\delta n_{\tau}(\mathbf{r}', t')$.

From a practical point of view, Eq. (21) has important and beneficial consequences. First, one is typically interested in using it for v_{xc} approximations whose dependence on the orbitals is analytically known. The functional derivatives in Eqs. (20) and (21) can thus also be calculated analytically. Second, if one uses the Sternheimer scheme for one's TDDFT calculations, then the linear response of the orbitals is calculated anyway. Therefore, evaluating Eqs. (20) and (21) is equivalent to, but much simpler than, actually calculating the kernel of an orbital-dependent potential. Thus, when one wants to stay on the grounds of Kohn-Sham theory, then the Sternheimer scheme for orbital functionals is much easier to use than the usual Casida [69] linear-response formalism.

III. LINEARIZATION OF THE ORBITAL-SPECIFIC POTENTIALS OF AN ORBITAL-ADIABATIC FUNCTIONAL

Typically, one is interested in the situation that one knows an orbital-dependent expression $E_{xc}[\{\varphi_{k\alpha}, \varphi_{k\alpha}^*\}]$ for the xc energy of GS DFT, based on which one can define a TDDFT action functional in an orbital-adiabatic fashion [35,48]. In the following, we demonstrate how the most common approximations to the TDOEP can be evaluated in the Sternheimer scheme.

A key ingredient in the TDOEP (and in its approximations) are the orbital-specific potentials $u_{xci\sigma}$, which in the orbital-adiabatic case are given by

$$u_{xci\sigma}(\mathbf{r}, t) = u_{xci\sigma}(\mathbf{r}) \Big|_{\substack{\varphi_{k\alpha} = \varphi_{k\alpha}(t), \\ \varphi_{k\alpha}^* = \varphi_{k\alpha}^*(t)}}, \quad (22)$$

where

$$u_{xci\sigma}(\mathbf{r}) = \frac{1}{\varphi_{i\sigma}^*(\mathbf{r})} \frac{\delta E_{xc}[\{\varphi_{k\alpha}, \varphi_{k\alpha}^*\}]}{\delta \varphi_{i\sigma}(\mathbf{r})}. \quad (23)$$

The goal of this section is to derive an expression for their linear response. We will then use this in Sec. IV. Since the $u_{xci\sigma}$ only depend on the orbitals at time t , we have

$$\frac{\delta u_{xci\sigma}(\mathbf{r}, t)}{\delta \varphi_{j\tau}(\mathbf{r}', t')} = \delta(t - t') \frac{\delta u_{xci\sigma}[\{\varphi_{k\alpha}, \varphi_{k\alpha}^*\}](\mathbf{r})}{\delta \varphi_{j\tau}(\mathbf{r}')} \Big|_{\substack{\varphi_{k\alpha} = \varphi_{k\alpha}(t), \\ \varphi_{k\alpha}^* = \varphi_{k\alpha}^*(t)}}. \quad (24)$$

The remaining functional derivative, evaluated at the zeroth-order orbitals $\varphi_{j\sigma}^{(0)}$ [as needed for Eqs. (20) and (21)], is in general neither real nor time independent since Eq. (8) shows that the $\varphi_{j\sigma}^{(0)}$ are still complex and time-dependent even for our real choice of the GS orbitals $\phi_{j\sigma}$. However, we will restrict

our theory to functionals that depend on the orbitals only via products $\varphi_{j\sigma}^*(\mathbf{r}, t) \cdot \varphi_{j\sigma}(\mathbf{r}', t)$, which includes functionals containing exact exchange contributions, self-interaction corrections without unitary orbital transformations [70,71], and kinetic-energy-dependent metageneralized gradient approximations. In that case,

$$\begin{aligned} & \left[\frac{\delta u_{xci\sigma}(\mathbf{r}, t)}{\delta \varphi_{j\tau}(\mathbf{r}', t')} \right]^{(0)} \\ &= \delta(t - t') \frac{\delta u_{xci\sigma}[\{\varphi_{k\alpha}, \varphi_{k\alpha}^*\}](\mathbf{r})}{\delta \varphi_{j\tau}(\mathbf{r}')} \Big|_{\substack{\varphi_{k\alpha} = \phi_{k\alpha} e^{-i\varepsilon_{k\alpha} t/\hbar}, \\ \varphi_{k\alpha}^* = \phi_{k\alpha}^* e^{+i\varepsilon_{k\alpha} t/\hbar}}} \\ &= \delta(t - t') e^{+i(\varepsilon_{j\tau}/\hbar)t} \frac{\delta u_{xci\sigma}[\{\varphi_{k\alpha}, \varphi_{k\alpha}^*\}](\mathbf{r})}{\delta \varphi_{j\tau}(\mathbf{r}')} \Big|_{\varphi_{k\alpha} = \varphi_{k\alpha}^* = \phi_{k\alpha}} \end{aligned} \quad (25)$$

and

$$\begin{aligned} & \left[\frac{\delta u_{xci\sigma}(\mathbf{r}, t)}{\delta \varphi_{j\tau}^*(\mathbf{r}', t')} \right]^{(0)} \\ &= \delta(t - t') e^{-i(\varepsilon_{j\tau}/\hbar)t} \frac{\delta u_{xci\sigma}[\{\varphi_{k\alpha}, \varphi_{k\alpha}^*\}](\mathbf{r})}{\delta \varphi_{j\tau}^*(\mathbf{r}')} \Big|_{\varphi_{k\alpha} = \varphi_{k\alpha}^* = \phi_{k\alpha}}. \end{aligned} \quad (26)$$

Note that during the functional differentiation we still have to treat $\varphi_{k\alpha}$ and $\varphi_{k\alpha}^*$ as independent and insert the real-valued GS orbitals $\phi_{k\alpha}$ only afterward. Also, while $\varphi_{k\alpha}$ and $\varphi_{k\alpha}^*$ enter the functional in a symmetric way, Eq. (23) shows that the $u_{xci\sigma}$ do not depend symmetrically on $\varphi_{k\alpha}$ and $\varphi_{k\alpha}^*$. Thus,

$$\frac{\delta u_{xci\sigma}(\mathbf{r})}{\delta \varphi_{j\tau}(\mathbf{r}')} \Big|_{\varphi_{k\alpha} = \varphi_{k\alpha}^* = \phi_{k\alpha}} \neq \frac{\delta u_{xci\sigma}(\mathbf{r})}{\delta \varphi_{j\tau}^*(\mathbf{r}')} \Big|_{\varphi_{k\alpha} = \varphi_{k\alpha}^* = \phi_{k\alpha}} \quad (27)$$

in general, even though those quantities are real. However,

$$\frac{\delta u_{xci\sigma}(\mathbf{r})}{\delta \varphi_{j\tau}(\mathbf{r}')} \Big|_{\varphi_{k\alpha} = \varphi_{k\alpha}^* = \phi_{k\alpha}} = \frac{\delta u_{xci\sigma}^*(\mathbf{r})}{\delta \varphi_{j\tau}^*(\mathbf{r}')} \Big|_{\varphi_{k\alpha} = \varphi_{k\alpha}^* = \phi_{k\alpha}} \quad (28)$$

and

$$\frac{\delta u_{xci\sigma}(\mathbf{r})}{\delta \varphi_{j\tau}^*(\mathbf{r}')} \Big|_{\varphi_{k\alpha} = \varphi_{k\alpha}^* = \phi_{k\alpha}} = \frac{\delta u_{xci\sigma}^*(\mathbf{r})}{\delta \varphi_{j\tau}(\mathbf{r}')} \Big|_{\varphi_{k\alpha} = \varphi_{k\alpha}^* = \phi_{k\alpha}} \quad (29)$$

still hold. In principle, we can use these relations and Eqs. (9) and (20) to construct the linear response of $u_{xci\sigma}^*(\mathbf{r}, t)$ to the perturbation, yielding

$$u_{xci\sigma}^{*(1)}(\mathbf{r}, t) = [u_{xci\sigma}^{(+)}(\mathbf{r}) e^{-i\omega t} + u_{xci\sigma}^{*(-)}(\mathbf{r}) e^{i\omega t}] e^{n t}, \quad (30)$$

where we have defined

$$\begin{aligned} u_{xci\sigma}^{(\pm)}(\mathbf{r}) &= \sum_{\tau} \sum_{j=1}^{N_{\tau}} \int d^3 r' \left\{ \frac{\delta u_{xci\sigma}^*(\mathbf{r})}{\delta \varphi_{j\tau}(\mathbf{r}')} \Big|_{\varphi_{k\alpha} = \varphi_{k\alpha}^* = \phi_{k\alpha}} \varphi_{j\tau}^{(\pm)}(\mathbf{r}') \right. \\ &+ \frac{\delta u_{xci\sigma}(\mathbf{r})}{\delta \varphi_{j\tau}(\mathbf{r}')} \Big|_{\varphi_{k\alpha} = \varphi_{k\alpha}^* = \phi_{k\alpha}} \varphi_{j\tau}^{(\mp)}(\mathbf{r}') \\ &\left. \pm i \left[\frac{\delta u_{xci\sigma}(\mathbf{r})}{\delta \varphi_{j\tau}(\mathbf{r}')} - \frac{\delta u_{xci\sigma}^*(\mathbf{r})}{\delta \varphi_{j\tau}^*(\mathbf{r}')} \right] \Big|_{\varphi_{k\alpha} = \varphi_{k\alpha}^* = \phi_{k\alpha}} \phi_{j\tau}(\mathbf{r}') \varepsilon_{j\tau}^{(+)} \right\}. \end{aligned} \quad (31)$$

However, most approximations to the TDOEP, such as the Slater and KLI potentials, only depend on the real parts of the orbital-specific potentials:

$$w_{xc\sigma}(\mathbf{r}, t) := \text{Re}[u_{xc\sigma}(\mathbf{r}, t)] = \frac{1}{2}[u_{xc\sigma}(\mathbf{r}, t) + u_{xc\sigma}^*(\mathbf{r}, t)]. \quad (32)$$

From the symmetries (28) and (29) it follows that

$$\left. \frac{\delta w_{xc\sigma}(\mathbf{r})}{\delta \varphi_{j\tau}(\mathbf{r}')} \right|_{\varphi_{k\alpha} = \varphi_{k\alpha}^* = \phi_{k\alpha}} = \left. \frac{\delta w_{xc\sigma}(\mathbf{r})}{\delta \varphi_{j\tau}^*(\mathbf{r}')} \right|_{\varphi_{k\alpha} = \varphi_{k\alpha}^* = \phi_{k\alpha}}, \quad (33)$$

and since the derivatives of $w_{xc\sigma}$ evaluated at the (real) GS orbitals $\phi_{k\alpha}$ are real, we also have [cf. Eq. (9)]

$$i\phi_{j\tau}(\mathbf{r}')\varepsilon_{j\tau}^{(1)}(t) \left. \frac{\delta w_{xc\sigma}(\mathbf{r})}{\delta \varphi_{j\tau}(\mathbf{r}')} \right|_{\varphi_{k\alpha} = \varphi_{k\alpha}^* = \phi_{k\alpha}} + \text{c.c.} = 0. \quad (34)$$

That means that if we now use Eq. (20) to calculate the linear response of $w_{xc\sigma}$, the $\varepsilon_{j\tau}^{(1)}(t)$ -dependent contributions to $\varphi_{j\sigma}^{(1)}(\mathbf{r}, t)$ cancel. Inserting the relations derived above as well as Eq. (9), we arrive at

$$w_{xc\sigma}^{(1)}(\mathbf{r}, t) = [w_{xc\sigma}^{(+)}(\mathbf{r})e^{-i\omega t} + \text{c.c.}]e^{nt}, \quad (35)$$

where

$$w_{xc\sigma}^{(+)}(\mathbf{r}) = \sum_{\tau} \sum_{j=1}^{N_{\tau}} \int d^3 r' \left. \frac{\delta w_{xc\sigma}(\mathbf{r})}{\delta \varphi_{j\tau}(\mathbf{r}')} \right|_{\varphi_{k\alpha} = \varphi_{k\alpha}^* = \phi_{k\alpha}} \times [\varphi_{j\tau}^{(+)}(\mathbf{r}') + \varphi_{j\tau}^{(-)}(\mathbf{r}')] \quad (36)$$

(which is equal to $\frac{1}{2}[u_{xc\sigma}^{(+)}(\mathbf{r}) + u_{xc\sigma}^{(-)}(\mathbf{r})]$) and

$$\delta w_{xc\sigma}(\mathbf{r})/\delta \varphi_{j\tau}(\mathbf{r}') = \frac{\delta}{\delta \varphi_{j\tau}(\mathbf{r}')} \frac{1}{2} \left[\frac{\delta E_{xc}[\{\varphi_{k\alpha}, \varphi_{k\alpha}^*\}]}{\varphi_{i\sigma}^*(\mathbf{r})\delta \varphi_{i\sigma}(\mathbf{r})} + \frac{\delta E_{xc}[\{\varphi_{k\alpha}, \varphi_{k\alpha}^*\}]}{\varphi_{i\sigma}(\mathbf{r})\delta \varphi_{i\sigma}^*(\mathbf{r})} \right]. \quad (37)$$

In the following section, we will see that in the linear response of approximations to the TDOEP (including the CEDA), $w_{xc\sigma}^{(+)}$ plays a role similar to the one that $u_{xc\sigma}$ plays in the nonlinearized potentials.

IV. LINEARIZATION OF COMMON APPROXIMATIONS TO THE TDOEP

One of the most simple and rather crude approximations to the (TD)OEP is the Slater potential. It is the orbital density-weighted average of the orbital-specific potentials [72,73],

$$v_{xc\sigma}^{\text{Sla}}(\mathbf{r}, t) = \sum_{i=1}^{N_{\sigma}} \frac{|\varphi_{i\sigma}(\mathbf{r}, t)|^2}{n_{\sigma}(\mathbf{r}, t)} w_{xc\sigma}(\mathbf{r}, t). \quad (38)$$

A more sophisticated and probably the most commonly known and employed approximation is the KLI potential [35,48,52]

$$v_{xc\sigma}^{\text{KLI}}(\mathbf{r}, t) = v_{xc\sigma}^{\text{Sla}}(\mathbf{r}, t) + \sum_{i=1}^{N_{\sigma}} \frac{|\varphi_{i\sigma}(\mathbf{r}, t)|^2}{n_{\sigma}(\mathbf{r}, t)} \times [v_{ii\sigma}^{\text{KLI}}(t) - w_{ii\sigma}(t)], \quad (39)$$

where

$$v_{ij\sigma}^{\text{KLI}}(t) := \int \varphi_{i\sigma}^*(\mathbf{r}, t) v_{xc\sigma}^{\text{KLI}}(\mathbf{r}, t) \varphi_{j\sigma}(\mathbf{r}, t) d^3 r, \quad (40)$$

$$w_{ij\sigma}(t) := \int \varphi_{i\sigma}^*(\mathbf{r}, t) w_{xc\sigma}(\mathbf{r}, t) \varphi_{j\sigma}(\mathbf{r}, t) d^3 r \quad (41)$$

are the matrix elements of $v_{xc\sigma}^{\text{KLI}}$ and $w_{xc\sigma}$ between the TD Kohn-Sham orbitals. At least for the special case of the exact exchange functional, a further approximation is known. The CEDA potential [53,54,74,75] is defined by

$$v_{xc\sigma}^{\text{CEDA}}(\mathbf{r}, t) = v_{xc\sigma}^{\text{Sla}}(\mathbf{r}, t) + \sum_{i,j=1}^{N_{\sigma}} \frac{1}{2} \left\{ \frac{\varphi_{i\sigma}(\mathbf{r}, t) \varphi_{j\sigma}^*(\mathbf{r}, t)}{n_{\sigma}(\mathbf{r}, t)} \times [v_{ij\sigma}^{\text{CEDA}}(t) - u_{ij\sigma}(t)] + \text{c.c.} \right\}, \quad (42)$$

where $v_{ij\sigma}^{\text{CEDA}}(t)$ and $u_{ij\sigma}(t)$ are defined similarly to $v_{ij\sigma}^{\text{KLI}}(t)$ and $w_{ij\sigma}(t)$, but with $v_{xc\sigma}^{\text{KLI}}(\mathbf{r}, t)$ and $w_{xc\sigma}(\mathbf{r}, t)$ replaced by $v_{xc\sigma}^{\text{CEDA}}(\mathbf{r}, t)$ and $u_{xc\sigma}(\mathbf{r}, t)$, respectively. If the sums in the KLI and CEDA expressions are allowed to run over all occupied orbitals, then the potentials are defined only up to a TD constant. This constant is usually fixed by the condition

$$v_{N_{\sigma}N_{\sigma}\sigma}^{\text{KLI,CEDA}}(t) - w_{N_{\sigma}N_{\sigma}\sigma}(t) = 0. \quad (43)$$

In practice, realizing the condition amounts to dropping the $i = N_{\sigma}$ term of the second (primed) sum in the KLI expression and the $i = j = N_{\sigma}$ term of the primed sum in the CEDA potential. This is indicated by the primes.

The Slater potential is an explicit orbital functional and can thus be linearized by a straightforward application of Eq. (21). With the help of Eqs. (35) and (36) we arrive at

$$v_{xc\sigma}^{\text{Sla}(1)}(\mathbf{r}, t) = [v_{xc\sigma}^{\text{Sla}(+)}(\mathbf{r})e^{-i\omega t} + \text{c.c.}]e^{nt}, \quad (44)$$

with

$$v_{xc\sigma}^{\text{Sla}(+)}(\mathbf{r}) = \sum_{i=1}^{N_{\sigma}} \left\{ \frac{\varphi_{i\sigma}^2(\mathbf{r})}{n_{\sigma}(\mathbf{r})} w_{xc\sigma}^{(+)}(\mathbf{r}) - \frac{n_{ii\sigma}^{(+)}(\mathbf{r})}{n_{\sigma}(\mathbf{r})} \Delta v_{i\sigma}^{\text{Sla}}(\mathbf{r}) \right\}. \quad (45)$$

Here we have defined

$$n_{ij\sigma}^{(+)}(\mathbf{r}) := \frac{1}{2} \{ \phi_{i\sigma}(\mathbf{r}) [\varphi_{j\sigma}^{(+)}(\mathbf{r}) + \varphi_{j\sigma}^{(-)}(\mathbf{r})] + \phi_{j\sigma}(\mathbf{r}) [\varphi_{i\sigma}^{(+)}(\mathbf{r}) + \varphi_{i\sigma}^{(-)}(\mathbf{r})] \}, \quad (46)$$

and

$$\begin{aligned} \Delta v_{i\sigma}^{\text{Sla}}(\mathbf{r}) &:= [v_{xc\sigma}^{\text{Sla}}(\mathbf{r}) - u_{xc\sigma}(\mathbf{r})]_{\varphi_{k\alpha} = \varphi_{k\alpha}^* = \phi_{k\alpha}} \\ &= [v_{xc\sigma}^{\text{Sla}}(\mathbf{r}) - u_{xc\sigma}^*(\mathbf{r})]_{\varphi_{k\alpha} = \varphi_{k\alpha}^* = \phi_{k\alpha}} \\ &= [v_{xc\sigma}^{\text{Sla}}(\mathbf{r}) - w_{xc\sigma}(\mathbf{r})]_{\varphi_{k\alpha} = \varphi_{k\alpha}^* = \phi_{k\alpha}} \end{aligned} \quad (47)$$

is simply the difference of the real-valued GS Slater and orbital-specific potentials. The diagonals of the symmetric matrix $n_{ij\sigma}^{(+)}(\mathbf{r}) = n_{ji\sigma}^{(+)}(\mathbf{r})$ reduce to the response components $n_{ii\sigma}^{(+)}(\mathbf{r}) = \phi_{i\sigma}(\mathbf{r}) [\varphi_{i\sigma}^{(+)}(\mathbf{r}) + \varphi_{i\sigma}^{(-)}(\mathbf{r})]$ of the orbital densities. In addition, $w_{xc\sigma}^{(+)}$ is the quantity derived in Sec. III and depends on the chosen xc functional through Eq. (37).

The linearization of the KLI and CEDA potentials is slightly more involved since they are only defined semiexplicitly by Eqs. (39) and (42) due to the appearance of their matrix elements on the right-hand sides of these equations. There are two different ways to deal with this problem, which however lead to the same result. The longer way is detailed in Appendix B. For a relatively short derivation one can simply linearize Eqs. (39) and (42) by expanding every input quantity into a perturbation series up to first order. Since these input quantities are known in terms of the Kohn-Sham orbitals, the expansions can be constructed using Eq. (20). Then the only remaining unknown terms are the first- and zeroth-order contributions to the KLI or CEDA potential. Equating only zeroth-order terms simply yields the GS KLI or CEDA equations and equating the first-order terms leads to the equations for the response $v_{xc\sigma}^{\text{KLI,CEDA}(1)}(\mathbf{r}, t)$ of the KLI or CEDA potential.

The resulting equations are

$$v_{xc\sigma}^{\text{KLI,CEDA}(1)}(\mathbf{r}, t) = [v_{xc\sigma}^{\text{KLI,CEDA}(+)}(\mathbf{r})e^{-i\omega t} + \text{c.c.}]e^{\eta t} \quad (48)$$

[consistent with Eq. (13)], with

$$\begin{aligned} & v_{xc\sigma}^{\text{KLI}(+)}(\mathbf{r}) \\ &= \sum_{i=1}^{N_\sigma} \left\{ \frac{\phi_{i\sigma}^2(\mathbf{r})}{n_\sigma(\mathbf{r})} w_{xc\sigma}^{(+)}(\mathbf{r}) - \frac{n_{ii\sigma}^{(+)}(\mathbf{r})}{n_\sigma(\mathbf{r})} \Delta v_{i\sigma}^{\text{KLI}}(\mathbf{r}) \right\} \\ &+ \sum_{i=1}^{N_\sigma'} \left\{ \frac{n_{ii\sigma}^{(+)}(\mathbf{r})}{n_\sigma(\mathbf{r})} \Delta v_{i\sigma}^{\text{KLI}} + \frac{\phi_{i\sigma}^2(\mathbf{r})}{n_\sigma(\mathbf{r})} \right. \\ &\left. \times \left[v_{i\sigma}^{\text{KLI}(+)} - w_{i\sigma}^{(+)} + \int n_{ii\sigma}^{(+)}(\mathbf{r}') \Delta v_{i\sigma}^{\text{KLI}}(\mathbf{r}') d^3 r' \right] \right\} \end{aligned} \quad (49)$$

for the KLI case and

$$\begin{aligned} & v_{xc\sigma}^{\text{CEDA}(+)}(\mathbf{r}) \\ &= \sum_{i=1}^{N_\sigma} \left\{ \frac{\phi_{i\sigma}^2(\mathbf{r})}{n_\sigma(\mathbf{r})} w_{xc\sigma}^{(+)}(\mathbf{r}) - \frac{n_{ii\sigma}^{(+)}(\mathbf{r})}{n_\sigma(\mathbf{r})} \Delta v_{i\sigma}^{\text{CEDA}}(\mathbf{r}) \right\} \\ &+ \sum_{i,j=1}^{N_\sigma'} \left\{ \frac{n_{ij\sigma}^{(+)}(\mathbf{r})}{n_\sigma(\mathbf{r})} \Delta v_{ij\sigma}^{\text{CEDA}} + \frac{\phi_{i\sigma}(\mathbf{r})\phi_{j\sigma}(\mathbf{r})}{n_\sigma(\mathbf{r})} \right. \\ &\left. \times \left[v_{ij\sigma}^{\text{CEDA}(+)} - w_{ij\sigma}^{(+)} + \int n_{ij\sigma}^{(+)}(\mathbf{r}') \Delta v_{ij\sigma}^{\text{CEDA}}(\mathbf{r}') d^3 r' \right] \right\} \end{aligned} \quad (50)$$

for the CEDA, where $\Delta v_{i\sigma}^{\text{KLI,CEDA}}(\mathbf{r})$ are defined equivalently to $\Delta v_{i\sigma}^{\text{Sla}}(\mathbf{r})$ [Eq. (47)],

$$w_{ij\sigma}^{(+)} := \int \phi_{i\sigma}(\mathbf{r}) w_{xc\sigma}^{(+)}(\mathbf{r}) \phi_{j\sigma}(\mathbf{r}) d^3 r \quad (51)$$

are the matrix elements of $w_{xc\sigma}^{(+)}(\mathbf{r})$ between the GS orbitals, and $v_{ij\sigma}^{\text{KLI,CEDA}(+)}$ and $\Delta v_{ij\sigma}^{\text{KLI,CEDA}}$ are the corresponding matrix elements of $v_{xc\sigma}^{\text{KLI,CEDA}(+)}$ and $\Delta v_{i\sigma}^{\text{KLI,CEDA}}(\mathbf{r})$. As before, primes indicate that the $i = N_\sigma$ (KLI approximation) or $i = j = N_\sigma$ (CEDA) terms are missing in the sums, which is a direct result of enforcing the condition (43) in Eqs. (39) and (42). Using Eq. (20) again to expand this condition into a

perturbation series yields, to orders zero and one,

$$\Delta v_{N_\sigma N_\sigma \sigma}^{\text{KLI,CEDA}} = 0 \quad (52)$$

and

$$v_{N_\sigma N_\sigma \sigma}^{\text{KLI,CEDA}(+)} - w_{N_\sigma N_\sigma \sigma}^{(+)} + \int n_{N_\sigma N_\sigma \sigma}^{(+)}(\mathbf{r}) \Delta v_{N_\sigma \sigma}^{\text{KLI,CEDA}}(\mathbf{r}) d^3 r = 0. \quad (53)$$

The left-hand sides in these equations are exactly the terms dropped in the primed sums of Eqs. (49) and (50). The KLI and CEDA response potentials should meet these conditions, which can be used to check or even enhance the numerical accuracy of these potentials.

V. METHOD

Linear-response calculations in the Sternheimer scheme are performed as described in Ref. [58]. We recapitulate only the main aspects here. The frequency ω enters the scheme only as a parameter. By solving the full scheme for a single chosen value of ω , we obtain the change in the density to first order in the perturbation. From this we obtain observables, e.g., the frequency-dependent dipole moment, evaluated at our single chosen frequency. From the solutions for various different ω values within a frequency range of interest, we can then construct a spectrum. Here η is a real parameter that determines the width of the Lorentzian lines in these spectra. Larger values of η accelerate convergence. Since the potential response $v_{\text{Hxc}\sigma}^{(+)}$ entering the right-hand side of the Sternheimer equations depends on their solutions, the scheme is solved self-consistently. We use Anderson mixing [76] to stabilize the convergence of this self-consistency loop. In every self-consistency step, Eq. (16) is solved with the complex symmetric conjugate gradient algorithm (CGsymm) introduced in Ref. [58].

To calculate photoabsorption spectra, we use the dipole approximation

$$v_{\text{ext},\sigma}^{(+)}(\mathbf{r}) = e\mathbf{r} \cdot \mathcal{E}^{(+)}, \quad (54)$$

where e is the elementary charge and $\mathcal{E}^{(+)}$ is a homogeneous electric field, and evaluate the induced dipole moment

$$\boldsymbol{\mu}^{(+)} = -e \int d^3 r \mathbf{r} n^{(+)}(\mathbf{r}) \quad (55)$$

from which we can deduce the polarizability $\underline{\alpha}(\omega)$ according to

$$\boldsymbol{\mu}^{(+)} = \underline{\alpha}(\omega) \cdot \mathcal{E}^{(+)}. \quad (56)$$

In general, three calculations with independent field directions are needed to construct the full polarizability tensor. Finally, the absorption cross section $\sigma(\omega)$ is calculated as

$$\sigma(\omega) = \frac{4\pi\omega}{3c} \text{Im}[\text{Tr}\underline{\alpha}(\omega)], \quad (57)$$

where c is the speed of light.

During a self-consistent Sternheimer linear-response calculation, after each solution of Eq. (16) we have to update $v_{xc\sigma}^{(+)}$ for a given set of response orbitals $\phi_{i\sigma}^{(\pm)}(\mathbf{r})$. For the Slater potential, this can be done by simply evaluating the

explicit expression (45). The expressions (49) and (50), however, are not explicit due to the matrix elements $v_{ij\sigma}^{\text{KLI,CEDA}(+)}$ appearing on the right-hand side. This is no major problem, though, as the KLI and CEDA potentials can be evaluated iteratively: For a given approximation to $v_{xc\sigma}^{\text{KLI,CEDA}(+)}(\mathbf{r})$, we can calculate approximate matrix elements and use them to construct a new approximation to $v_{xc\sigma}^{\text{KLI,CEDA}(+)}(\mathbf{r})$ from Eq. (49) or (50). This has to be repeated until self-consistency between the potentials used to calculate the matrix elements and those constructed from these elements is reached. During this procedure, the orbital-specific response potentials $w_{xci\sigma}^{(+)}(\mathbf{r})$ do not have to be iterated since they do not depend on the matrix elements. This means that they only have to be constructed once per Sternheimer self-consistency step, which is convenient since their construction involves the most time-consuming steps in the calculation of the Slater, KLI, or CEDA potential response: For EXX, they contain $N_{\sigma}(N_{\sigma} + 1)/2$ independent Fock integrals $\int e^2 n_{ij\sigma}^{(+)}(\mathbf{r}')/|\mathbf{r} - \mathbf{r}'|d^3r'$ per spin channel. This reduces to only N_{σ} diagonal self-Hartree integrals $\int e^2 n_{ii\sigma}^{(+)}(\mathbf{r}')/|\mathbf{r} - \mathbf{r}'|d^3r'$ for the self-interaction correction functional [77].

We have added the routines for the construction of the KLI and CEDA potential response to our Sternheimer linear-response code [58] in the Bayreuth version [78,79] of the PARSEC [80] GS program package, which employs a real-space grid and norm-conserving Troullier-Martins pseudopotentials [81,82].

In our implementation, the Coulomb integrals incorporated in $w_{xci\sigma}^{(+)}(\mathbf{r})$ are evaluated by solving Poisson's equation using multigrad techniques [21,83]. This is also how we calculate the response of the Hartree potential.

In every self-consistency step, the additional iteration that is needed to construct $v_{xc\sigma}^{\text{KLI,CEDA}(+)}(\mathbf{r})$ is stabilized by Anderson mixing and thus typically converges in roughly three to six (KLI approximation) or five to ten (CEDA) steps. During this iteration, only the numerically cheap one-point integrals for the matrix elements $v_{ij\sigma}^{\text{KLI,CEDA}(+)}$ have to be evaluated repeatedly, which is of negligible cost compared to solving Poisson's equation. Thus, the cost for constructing the response $v_{xc\sigma}^{(+)}(\mathbf{r})$ of the Slater, KLI, or CEDA potential once for a given set of response orbitals is roughly the same as for constructing the occupied orbital-specific response potentials $w_{xci\sigma}^{(+)}(\mathbf{r})$.

VI. RESULTS

In this section we present several applications involving the KLI and CEDA potential response, mainly to demonstrate that our method works and to prove that it is a useful addition to other TDDFT approaches like the Casida formalism or real-time propagation. To that purpose, we first consider in Sec. VIA a case that allows us to compare the detailed spatial structure of the xc potential response to reference calculations. We thus confirm that we are able to construct $v_{xc\sigma}^{(+)}(\mathbf{r})$ with high accuracy throughout the whole simulation sphere and even at large distances from the system.

In Sec. VIB, we then calculate absorption spectra for a system where we can also perform stable real-time propagations with KLI and CEDA potentials. By comparing the resulting spectra we show that our method works well through an

extended frequency range and therefore is a suitable alternative to the real-time method.

Finally, in Sec. VIC, we calculate the absorption spectrum for a system for which real-time propagations with KLI potentials are notoriously unstable. We thus provide a proof of concept that our method allows us to circumvent the stability issues that can arise in real-time calculations employing potentials which are not strictly defined as functional derivatives.

We focus on the KLI and CEDA potential of the exact exchange (XKLI and XCEDA, respectively) functional, defined as the Fock integral evaluated with Kohn-Sham orbitals, and on the KLI potential of the self-interaction-corrected local-density approximation (SICKLI) [29,70].

A. Hydrogen chain: Comparison to static finite-field results

To test our way of calculating the response of the xc potential, we do not want to rely solely on excitation spectra for two reasons. First, excitation energies are affected by the chosen xc approximation not only through the kernel or the potential response, but also through GS properties such as the Kohn-Sham eigenvalue spectrum or GS potential. It is therefore not straightforward to extract information “purely” on $v_{xc\sigma}^{(+)}(\mathbf{r})$ from excitation energies. The second problem is that “integrated” quantities such as dipole moments or the absorption cross section contain less information than the potential itself as a function of the spatial coordinates. Even a wrong kernel or potential response can by chance move the energies of some excitations in the right direction on the frequency axis, but potentially makes grave errors for other types of excitations. We would thus have to test our implementation for a large number of excitation energies of as many different excitation types (valence, Rydberg, charge transfer, etc.) as possible to make sure that the potential is calculated correctly.

Therefore, we follow a two-pronged approach. We test our method for excitation energy spectra (see the following sections), but we also directly examine the response potential as a function of the spatial coordinates in this section. For that purpose, we need a test case which should have two properties. The first is that different xc approximations should yield clearly different results for $v_{xc\sigma}^{(+)}(\mathbf{r})$. The second is that we should be able to construct the response of the potential for the xc approximations under consideration by some method that is different from and completely independent of our linear-response formalism and can thus serve as a benchmark for our response potential $v_{xc\sigma}^{(+)}(\mathbf{r})$.

The static field-counteracting effect in hydrogen chains meets these conditions: Hydrogen chains with alternating H-H distances of $2a_0$ and $3a_0$ (where a_0 is the Bohr radius) are frequently used model systems that provide a tough test case for many-body methods [71,84–94]. Local and standard semilocal functionals are known to severely overestimate the static polarizability and hyperpolarizabilities in these systems. This error is not removed but significantly reduced by the EXX, with the CEDA performing better than the KLI approximation and the exact OEP yielding the best results. Due to these pronounced differences, hydrogen chains make for ideal test systems and therefore we study the H_8 molecule in the following.

The observed differences have been traced back, at least partially, to an ultranlocal feature of the EXX potential which cannot be mimicked by standard semilocal functionals: When a system is placed in a homogeneous external field, the EXX GS potential builds up a field-counteracting term, which makes it harder to move charge and thus lowers the polarizability.

The standard way [74,85,88] to visualize this term is by performing two GS calculations. In the first one, the electrons are merely subjected to the atomic potentials. In the second one, an additional external potential

$$v_{\text{ext}}(\mathbf{r}) = e\mathcal{E}x \quad (58)$$

is applied. This corresponds to a homogeneous electric field of strength \mathcal{E} along the x direction. Then one simply plots the difference of the resulting xc potentials

$$\Delta v_{\text{xc}}(\mathbf{r}) := v_{\text{xc}}(\mathbf{r})|_{\mathcal{E} \neq 0} - v_{\text{xc}}(\mathbf{r})|_{\mathcal{E} = 0}. \quad (59)$$

In this way, the position-dependent response of the xc potential to the field can be constructed from two standard GS calculations, without the need for an explicit expression for $v_{\text{xc}\sigma}^{(+)}(\mathbf{r})$.

To make the connection to our linear-response scheme, we first treat the potential of the static external field as a small perturbation and expand $v_{\text{xc}}(\mathbf{r})$ around $\mathcal{E} = 0$. For small field strengths, this leads to

$$\Delta v_{\text{xc}}(\mathbf{r}) \xrightarrow{\mathcal{E} \rightarrow 0} v_{\text{xc}}^{(1)}(\mathbf{r}) + O(\mathcal{E}^2), \quad (60)$$

where $v_{\text{xc}}^{(1)}(\mathbf{r})$ is the static first-order response of the xc potential.

Next we examine the static limit of our TD Sternheimer scheme: For vanishing ω and η , the general TD perturbation introduced in Sec. II becomes time independent,

$$v_{\text{ext},\sigma}(\mathbf{r}, t) \xrightarrow{\omega, \eta \rightarrow 0} 2 \text{Re}[v_{\text{ext},\sigma}^{(+)}(\mathbf{r})]. \quad (61)$$

Thus, we can mimic the situation described above in a Sternheimer calculation by setting ω and η to zero and choosing the real-valued perturbation

$$v_{\text{ext},\sigma}^{(+)}(\mathbf{r}) = \frac{1}{2}e\mathcal{E}x. \quad (62)$$

Similarly, the TD linear response of the xc potential becomes time independent,

$$v_{\text{xc}\sigma}^{(1)}(\mathbf{r}, t) \xrightarrow{\omega, \eta \rightarrow 0} 2 \text{Re}[v_{\text{xc}\sigma}^{(+)}(\mathbf{r})]. \quad (63)$$

Since in this limit, and for a real perturbation, $v_{\text{xc}\sigma}^{(+)}$ also becomes real, we can simply evaluate Δv_{xc} as

$$\Delta v_{\text{xc}}(\mathbf{r}) = 2v_{\text{xc}\sigma}^{(+)}(\mathbf{r}) \quad (64)$$

after performing a self-consistent Sternheimer calculation with the $v_{\text{ext},\sigma}^{(+)}$ given above and with small or vanishing values for ω and η . Comparing the resulting $\Delta v_{\text{xc}}(\mathbf{r})$ with the one calculated from Eq. (59) after two GS calculations thus allows us to probe directly the full spatial structure of our $v_{\text{xc}\sigma}^{(+)}(\mathbf{r})$ construction and to compare it to an independent reference. (In this way we check the full spatial structure of the response, whereas the frequency dependence will be checked in the following sections.)

We have performed these tests for the XKLI, XCEDA, and SICKLI potential [95]. To make sure that our static finite-field calculations are well within the linear regime, which is required so that the results from Eqs. (59) and (64) can coincide, we use an extremely small field strength of $\mathcal{E} = 10^{-6} e/a_0^2$.

Also, since the frequency ω enters the Sternheimer scheme merely as a parameter, it should in principle be sufficient to test our implementation for $\omega = 0$ in order to verify that our method is correct. However, $\omega = \eta = 0$ might be a special case numerically. Therefore, we here present results for small but nonvanishing values of $\hbar\omega = 0.2$ eV and $\hbar\eta = 0.1$ meV. This should make it easier to conclude that if our method works well for these parameter values, it should in principle also do so for any other value. Additionally, we explicitly checked that doing the calculations for $\omega = \eta = 0$ poses no problem and yields virtually the same results as for these finite values.

Figure 1 shows our results for the various functionals. For comparison, we also include the LDA potential response. One can clearly see the field-enhancing character of the LDA, the well-known field-counteracting behavior of the EXX, which is slightly more pronounced in the CEDA than in the KLI potential, as well as the lack thereof for the SICKLI potential. (We here once more note that for the SIC energy functional, the details of how the potential is constructed are very important, as discussed previously in Refs. [29,71,94].) More interesting for our purposes is that in all cases, the Sternheimer and finite-field results perfectly coincide not only qualitatively, but also quantitatively. This is true for the whole simulation sphere which extends out to $\pm 25a_0$, $16.5a_0$ beyond the outermost atom. In Appendix C we verify that the decisive features and the differences between the different functionals observed here do not follow just from differences in the ground-state eigenvalues or orbitals, but are really a consequence of differences in the exchange(-correlation) response.

B. Silane photoabsorption spectrum: Comparison to propagation results

After having shown in the preceding section that we can construct the response of the KLI and CEDA potentials correctly with its full spatial dependence for a given frequency, we now demonstrate that our approach works for different frequencies, i.e., we verify that our approach allows for calculating absorption spectra using orbital functionals within the Kohn-Sham framework. We thus prove in particular that no unexpected numerical problems arise when solving the Sternheimer scheme with the KLI or CEDA response for a frequency close to a resonance.

For this we need reference Kohn-Sham TDDFT calculations to compare to. As discussed in the Introduction, the number of orbital functional calculations reported in the literature using the Kohn-Sham approach is limited. Furthermore, it makes sense to base the comparison on reference data that are completely independent, but technically and in accuracy comparable to our real-space approach. For these reasons, silane (SiH_4) appears as an ideal test system, because for this molecule, real-space, real-time propagation linear-response calculations using the XKLI and SICKLI potentials

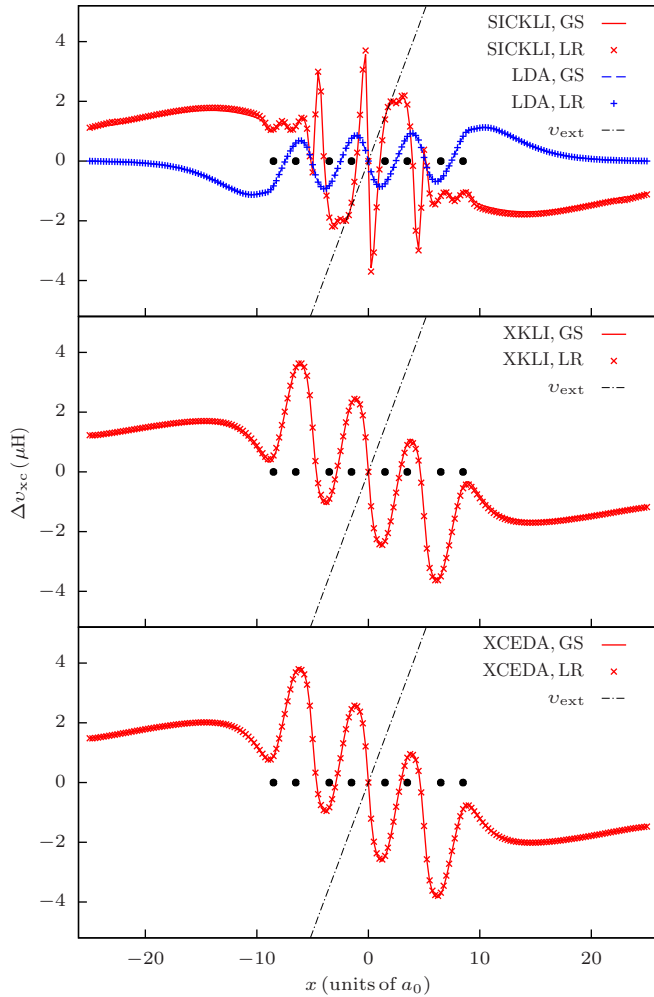


FIG. 1. Static response $\Delta v_{xc}(\mathbf{r})$ of the xc potential to an external electric field for the H_8 model and $\mathcal{E} = 10^{-6} e/a_0^2$. Lines are constructed from GS calculations and Eq. (59), while points are the results from Sternheimer linear-response calculations and Eq. (64). Black circles mark the positions of the H atoms.

have been reported [18,21,29]. In order to have a full set of accurate reference data available for comparison we calculated the photoabsorption spectrum of SiH_4 ourselves once more by real-time propagation for the XKLI, XCEDA, and SICKLI potentials using the BTDF program package [96].

We compare this reference data to the KLI and CEDA photoabsorption spectra that we calculate with the Sternheimer scheme. In the latter, we use the XKLI approximation (or XCEDA or SICKLI approximation, respectively) throughout the full calculation, i.e., both in the GS calculation and for the construction of $v_{xc}^{(+)}(\mathbf{r})$. For the comparison we focus on the energy range in which the most important excitations lie, which is between 8 and 13 eV for the EXX potentials XKLI and XCEDA, and between 7.3 and 11.8 eV for the SICKLI potential. The results for XKLI, XCEDA, and SICKLI potentials are shown in Figs. 2(a), 2(b), and 2(c), respectively [97].

In all three cases, the real-time and Sternheimer spectra with corresponding xc approximations agree perfectly. This confirms our method of linearizing the KLI and CEDA potentials.

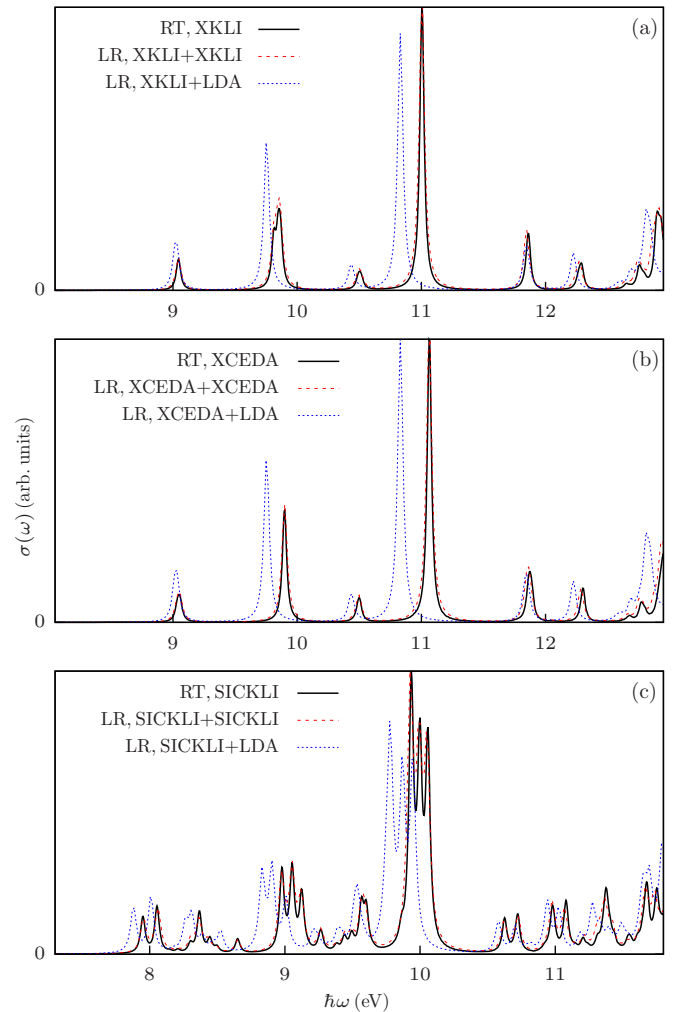


FIG. 2. Photoabsorption spectra of SiH_4 calculated with different xc approximations. Red dashed lines marked LR show results from Sternheimer linear-response calculations in which the same xc approximation has been used for the ground-state calculation and the calculation of the response potential, namely, (a) exact exchange in the KLI approximation, (b) exact exchange in the CEDA, and (c) the SICKLI potential. Black solid lines marked RT denote the results from real-time propagations as a reference. The agreement is excellent. Blue dotted lines show results from Sternheimer linear-response calculations in which the ground-state calculation was done as previously, but the LDA was used for constructing the response potential. This shifts the excitation energies noticeably.

Finally, we perform linear-response calculations where again the KLI or CEDA potentials for the EXX and SIC functionals are used in the GS calculation, but $v_{xc}^{(+)}(\mathbf{r})$ is constructed from the LDA. In this way, we can check how sensitive the photoabsorption calculation is to the xc approximation that is used for computing the response potential. Using the LDA potential response on top of the orbital functional ground states leads to excitation energies that are shifted by 0.1–0.3 eV, i.e., notable differences. Thus, the response potential does influence the excitation energies and the agreement observed above is not trivial.

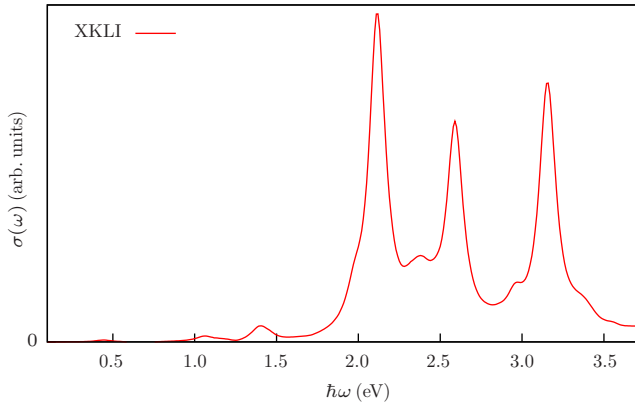


FIG. 3. The XKLI photoabsorption spectrum of Na_5 .

C. Photoabsorption in Na_5 : The Sternheimer approach for a system where real-time propagation is unstable

Finally, we demonstrate in the following that the Sternheimer approach allows us to examine cases that cannot be described properly by the real-time approach. When an xc potential approximation is used that is not a functional derivative, the real-time propagation of the Kohn-Sham equations can become unstable. This has been demonstrated explicitly, e.g., for the XKLI potential [55] and other approximations [98]. The violation of the zero-force theorem [99,100] has been suggested as an explanation of this effect [55].

The Sternheimer linear-response approach offers the possibility to avoid such instabilities, as the time dependence of the density, orbitals, and Kohn-Sham potential has been constructed analytically, and one only has to find the Fourier components for various frequencies. These frequencies are independent of each other. Thus, whereas instabilities can build up from time step to time step in a real-time propagation, no instabilities can build up when going from frequency to frequency. Therefore, the Sternheimer formalism can yield stable converged results even for systems where propagations become unstable.

The sodium cluster Na_5 has become infamous for being a system where propagations with various xc potentials including XKLI and SICKLI have been reported to become unstable and the zero-force violations have been found to be severe [20,29,55,56,98,101]. We therefore focus on this system as a worst-case scenario.

We use the TURBOMOLE [102] program package to optimize the Na_5 geometry at the B3LYP/def2-QZVPP [3,103,104] level. Then we calculate the XKLI photoabsorption spectrum as described in Sec. V. Figure 3 shows our results [105]. While both the GS and the linear-response self-consistency iterations take more steps to converge than for other sodium clusters of comparable size or for silane, we do not encounter any serious problems in the calculations.

In real-time calculations with a stable propagation, the total propagation time only governs the linewidths. Due to the instabilities arising in the Na_5 calculations, however, the spectrum changes qualitatively with increasing propagation time: New lines appear, grow in intensity, and move along the frequency axis. This makes it impossible to uniquely identify excitation energies or oscillator strengths.

Therefore, we carefully examine whether our Sternheimer spectrum is unique and robust with respect to numerical parameters. The parameter determining the linewidths in our approach, and in that sense “corresponding” to the total propagation time, is η . Calculations with various different values for η show that it indeed only influences the shape, but not the number, positions, or heights of the lines in the spectrum, as it should.

Additionally, we tested how the atomic coordinates, the numerical grid, and the convergence criteria in the linear-response algorithm influence the calculation. Switching from our coordinates to the MP2/6-31G(d)-optimized coordinates presented in Ref. [106] only leads to an almost rigid redshift of the whole spectrum by approximately 0.1 eV. Using a larger simulation sphere radius, a smaller spacing of the numerical grid, or stricter convergence criteria has almost no noticeable influence on the spectrum. Switching to the unoccupied subspace projection scheme presented in Appendix A also has no effect on the resulting spectrum. Finally, in Appendix D we verify that our XKLI spectrum is physically reasonable by comparing it to reference calculations and to experiment.

All of this leads to the conclusion that the Sternheimer linear-response approach indeed allows us to construct a unique, converged, and robust XKLI photoabsorption spectrum for Na_5 .

VII. CONCLUSION

We have derived an approach that enables one to use the KLI approximation and the CEDA in the time-dependent Kohn-Sham scheme in a computationally efficient and numerically stable way. Our approach inherits the computational advantages of the general Sternheimer scheme that have been discussed in previous works [57,58]: No unoccupied orbitals need to be calculated, the approach scales well because adding an electron just adds one more response equation to be solved, and the structure of the equations is such that they can very efficiently be parallelized. In our work, a numerical grid is used for solving the equations, but a basis set implementation is possible as well. Based on the frequency-dependent Sternheimer formalism, we derived a set of transparent equations for the density response in which the frequency of the excitation enters just as a parameter. A linear-response spectrum can thus easily be generated for an orbital functional in the KLI approximation or the CEDA over a wide range of frequencies in a massively parallel computation by solving the equations independently for each frequency. We have demonstrated the stability and accuracy of this orbital-Sternheimer scheme for well-established test cases. In contrast to the real-time propagation approach in which the errors introduced by the KLI or CEDA potential (both being only approximate solutions to the true functional derivative defined by the OEP) can accumulate from time step to time step, no error accumulation can occur in the separate calculations for each frequency.

The derivation of this scheme led to the important insight that the linear response of an orbital functional can be obtained within the Kohn-Sham framework *without* having to compute the xc kernel f_{xc} explicitly. Instead, the Kohn-Sham response in our scheme is obtained from expressions that involve only functional derivatives with respect to the orbitals.

The latter can straightforwardly be obtained in an analytical calculation for a given density functional. Thus, two notorious limitations that hindered the use of orbital functionals in time-dependent Kohn-Sham theory, the instability of the nonlinearized equations under the KLI approximation and the CEDA, and the construction of f_{xc} , which is analytically and numerically involved for orbital functionals, have been overcome.

The obvious challenge that remains is to extend the present approach beyond the KLI approximation and the CEDA into a full time-dependent OEP scheme. Despite the progress made in this work, this is still a formidable task. The orbital shift terms that make the difference between, e.g., the KLI potential and the true OEP [48], cannot be taken into account directly within the present scheme. Further work is needed to devise, e.g., an iterative correction scheme similar to the one that can be used for the ground state [107]. Such future work may then also be able to track down signatures of the KLI and CEDA instability in the linear-response signals. The present work thus serves as an important step towards the ultimate goal of being able to use orbital functionals without further approximations efficiently and reliably in the time-dependent Kohn-Sham framework, and it already enables such use within the KLI approximation and the CEDA, which have been demonstrated to be rather accurate in many cases of practical interest.

ACKNOWLEDGMENTS

We acknowledge financial support from the German-Israeli Foundation for Scientific Research and Development and the program ‘‘Biological Physics’’ of the Elite Network of Bavaria. We further acknowledge support through the computational resources provided by the Bavarian Polymer Institute and by the Bavarian State Ministry of Science, Research, and the Arts in the Collaborative Research Network ‘‘Solar Technologies go Hybrid.’’ F.H. acknowledges support from the University of Bayreuth Graduate School.

APPENDIX A: UNOCCUPIED SUBSPACE PROJECTION

It has been noted earlier that in the construction of the density response, the contributions to $\varphi_{j\sigma}^{(\pm)}$ proportional to occupied GS orbitals cancel [57,58]. Therefore, if the response of the orbitals is only needed to calculate $n_{\sigma}^{(+)}$, one can work with projections of the orbitals onto the unoccupied subspace

$$\tilde{\varphi}_{j\sigma}^{(\pm)}(\mathbf{r}) := \hat{Q}_{\sigma} \varphi_{j\sigma}^{(\pm)}(\mathbf{r}) \quad (\text{A1})$$

with the projector

$$\hat{Q}_{\sigma} := \prod_{j=1}^{N_{\sigma}} \hat{Q}_{j\sigma} = 1 - \sum_{j=1}^{N_{\sigma}} |\phi_{j\sigma}\rangle \langle \phi_{j\sigma}|. \quad (\text{A2})$$

In this work, however, we are dealing with quantities that depend directly on the orbitals instead of only on the density. For these quantities, the occupied contributions do not have to cancel, so we actually need the full orbitals $\varphi_{j\sigma}^{(\pm)}$.

If we expand these with respect to the GS orbitals

$$\varphi_{j\sigma}^{(\pm)}(\mathbf{r}) = \sum_{k \neq j} c_{jk\sigma}^{(\pm)} \phi_{k\sigma}(\mathbf{r}) \quad (\text{A3})$$

(where we have already exploited the orthogonality of $\varphi_{j\sigma}^{(\pm)}$ and $\phi_{j\sigma}$), then the solution to the Sternheimer equations (16) for a fixed right-hand side (i.e., in a single step of the self-consistency iteration) is given by

$$c_{jk\sigma}^{(\pm)} = \frac{\langle \phi_{k\sigma} | v_{\text{ext},\sigma}^{(+)} + v_{\text{Hxc}\sigma}^{(+)} | \phi_{j\sigma} \rangle}{\varepsilon_{j\sigma} - \varepsilon_{k\sigma} \pm \hbar(\omega + i\eta)}. \quad (\text{A4})$$

While in general both occupied and unoccupied GS orbitals and eigenvalues are needed to calculate this expression, we obviously only need the occupied Kohn-Sham spectrum to construct the occupied contributions to $\varphi_{j\sigma}^{(\pm)}$. Thus, the full orbital response can be calculated as

$$\varphi_{j\sigma}^{(\pm)}(\mathbf{r}) = \tilde{\varphi}_{j\sigma}^{(\pm)}(\mathbf{r}) + \sum_{\substack{k=1 \\ k \neq j}}^{N_{\sigma}} \frac{\langle \phi_{k\sigma} | v_{\text{ext},\sigma}^{(+)} + v_{\text{Hxc}\sigma}^{(+)} | \phi_{j\sigma} \rangle \phi_{k\sigma}(\mathbf{r})}{\varepsilon_{j\sigma} - \varepsilon_{k\sigma} \pm \hbar(\omega + i\eta)}. \quad (\text{A5})$$

Acting with \hat{Q}_{σ} on Eq. (16) yields

$$\begin{aligned} & [\hat{h}_{\sigma} - \varepsilon_{j\sigma} \mp \hbar(\omega + i\eta)] \tilde{\varphi}_{j\sigma}^{(\pm)}(\mathbf{r}) \\ &= -\hat{Q}_{\sigma} [v_{\text{ext},\sigma}^{(+)}(\mathbf{r}) + v_{\text{Hxc}\sigma}^{(+)}(\mathbf{r})] \phi_{j\sigma}(\mathbf{r}), \end{aligned} \quad (\text{A6})$$

which differs from the original Sternheimer equation only in that $\hat{Q}_{j\sigma}$ is replaced by \hat{Q}_{σ} . Finally, by construction,

$$\langle \phi_{k\sigma} | \tilde{\varphi}_{j\sigma}^{(\pm)} \rangle = 0 \quad \forall k \in \{1, \dots, N_{\sigma}\}. \quad (\text{A7})$$

These equations fully determine $\varphi_{j\sigma}^{(\pm)}$. If we replace the Sternheimer equation (16) by solving the set of equations given above in every self-consistency step, then instead of the full response orbitals, only their unoccupied subspace projections have to be constructed from a conjugate gradient scheme while the occupied contributions are calculated exactly. This can potentially lead to a higher numerical accuracy in the resulting $\varphi_{j\sigma}^{(\pm)}$.

The accuracy of the response orbitals can become particularly important when KLI or CEDA potentials are linearized with the method presented in Sec. IV due to the occurrence of terms like $\frac{n_{j\sigma}^{(+)}(\mathbf{r})}{n_{\sigma}(\mathbf{r})}$, where basically the response of the orbitals is divided by the GS density. Since the density falls off exponentially outside the system, inaccuracies in the $\varphi_{j\sigma}^{(\pm)}$ can easily lead to artificial divergences in the response potential.

We illustrate this for the H_8 system investigated in Sec. VIA: When solving the Sternheimer equation (16) or (A6) with the CGsymm algorithm, we reduce the residual norm by a factor of 10^{ρ} . For calculations with the LDA we often find $\rho = 6$ to be enough to arrive at well-converged, physically meaningful results, but for the KLI and CEDA potentials this convergence criterion turns out to be too weak. Therefore, the calculations in Sec. VIA were done with $\rho = 8$. When we repeat these calculations with $\rho = 6$, we find that the LDA results do not change at all. In Fig. 4, however, we show that the XKLI potential response now indeed is erroneously diverging towards the border of our simulation

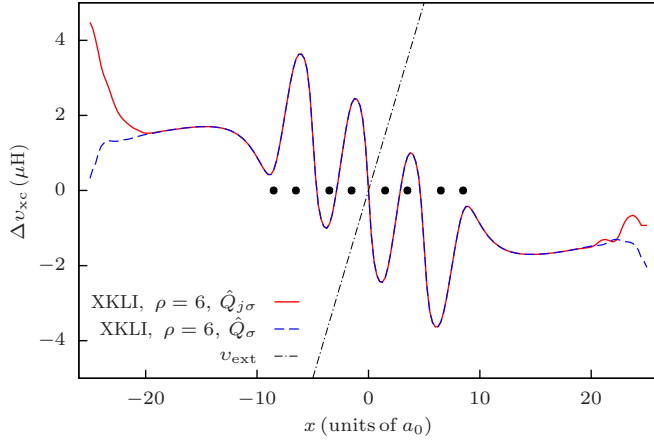


FIG. 4. Linear-response results for $\Delta v_{xc}(\mathbf{r})$ calculated from Eq. (64) with the XKLI potential and a weak CGSymm convergence criterion of $\rho = 6$. The red solid line is based on the Sternheimer equation (16) (designated by the projector $\hat{Q}_{j\sigma}$ appearing in that equation) and the blue dashed line is based on the projector method (A6) (\hat{Q}_σ).

sphere, beginning at a distance of approximately $19a_0$ from the system's center.

The number of self-consistency steps needed for the full calculation is also influenced by these inaccuracies occurring in every single step: With $\rho = 8$, we usually need seven to eight steps to converge the self-consistency iteration, independently of whether we are using exactly vanishing or small but finite values for ω and η and of whether we are working with the XKLI, XCEDA, or SICKLI potential. With $\rho = 6$, however, the XKLI calculation presented in Fig. 4 needed 18 steps to converge.

Both of these deficiencies are affected if we switch from using the “original” Sternheimer equation (16) to the unoccupied subspace projection scheme presented above [i.e., Eq. (A6)]. As can be seen from Fig. 4, the divergent behavior of $v_{xc}^{(+)}(\mathbf{r})$ is reduced but not eliminated. The potential response still diverges, but less seriously, and it starts doing so only slightly further outside the system, at approximately $22a_0$. More interestingly, the self-consistency process is strongly stabilized, with the number of self-consistency iteration steps needed to converge now being reduced again to 8. Thus, in this case of a too-weak CGsymm convergence criterion, the projector method is significantly more effective than the unprojected Sternheimer scheme.

However, since the method cannot completely repair the errors in the response potential that result from an inaccurate solution of the Sternheimer equations in every self-consistency step, we recommend always choosing a sufficiently strong convergence criterion. Additionally, the projector scheme can be applied as a safety net to ensure stability of the self-consistency process. Also, since the results with and without the projector can only differ if the Sternheimer equations are not solved rigorously enough, comparing results from calculations with the two different schemes can be a useful test. We use this to verify that the spectra presented in Secs. VI B and VI C, calculated with $\rho = 10$ and $\rho = 12$, respectively, are indeed accurate.

APPENDIX B: ALTERNATIVE DERIVATION OF THE LINEARIZATION OF THE KLI AND CEDA POTENTIALS

In this appendix we discuss an alternative derivation of Eqs. (48)–(50). We start by noting that even though Eqs. (39) and (42) are not explicit expressions for the potentials $v_{xc\sigma}^{\text{KLI,CEDA}}(\mathbf{r}, t)$, they do allow one to calculate these potentials once the occupied orbitals are known. Therefore, $v_{xc\sigma}^{\text{KLI,CEDA}}(\mathbf{r}, t)$ can still be seen as implicit orbital functionals and can thus formally be linearized by means of Eq. (21). As the orbital dependence is only implicit, the functional derivatives with respect to the orbitals needed for this approach are not calculated analytically. Instead, one can take the derivative of Eq. (39) or (42). Since all input quantities for these equations except for the potentials themselves are known explicitly in terms of the orbitals, this leads to equations determining the unknown functional derivatives $\delta v_{xc\sigma}^{\text{KLI,CEDA}}(\mathbf{r}, t)/\delta\varphi_{j\tau}(\mathbf{r}', t')$. It would be impractical to try to solve these equations directly on a real-space grid since the functional derivatives depend on two spatial variables, i.e., they would be represented by (possibly dense) matrices on the grid. Instead, every operation that has to be performed on the functional derivatives to construct the response potential according to Eq. (21) (i.e., the multiplication with the orbital response, addition of the complex conjugate, summation over the orbitals, and integration) can be applied directly to the equations for the derivatives. Rearranging the resulting equations and inserting Eq. (21) finally leads to equations directly determining the linear response of the potentials $v_{xc\sigma}^{\text{KLI,CEDA}}(\mathbf{r}, t)$ [cf. Eqs. (48)–(50)], which can be solved on a grid.

APPENDIX C: CHECKING THE INFLUENCE OF THE GROUND-STATE ELECTRONIC STRUCTURE ON THE H₈ CHAIN RESPONSE

With the following test we verify that the large qualitative differences between the $\Delta v_{xc}(\mathbf{r})$ observed for the different functionals for H₈ are mostly due to the different functionals used to construct $v_{xc\sigma}^{(+)}(\mathbf{r})$ and not a consequence of differences in the underlying GS calculation. We perform this test because *a priori* one cannot rule out the possibility that at least a highly nonlocal functional such as EXX might be quite sensitive to small differences in the GS density and orbitals that enter the construction of $v_{xc\sigma}^{(+)}(\mathbf{r})$.

Thus, one could speculate that the perfect agreement between our GS and Sternheimer results might only partially be due to our correct construction of $v_{xc\sigma}^{(+)}(\mathbf{r})$ and in another part simply reflect that we are using the correct GS quantities. If that were the case, then our test of the response would not be as stringent as hoped. However, as demonstrated here, this possibility can be ruled out, i.e., the test reported in Fig. 1 is stringent.

As a cross-check we perform two additional linear-response calculations, using different xc approximations in the GS calculation and in the construction of $v_{xc\sigma}^{(+)}(\mathbf{r})$: Once we combine the GS of the LDA with the XKLI response (dubbed LDA+XKLI in Fig. 5) and once we use the opposite combination, i.e., the XKLI GS with the potential response of the LDA (XKLI+LDA). Figure 5 unambiguously shows that the LDA+XKLI and XKLI+LDA results are virtually

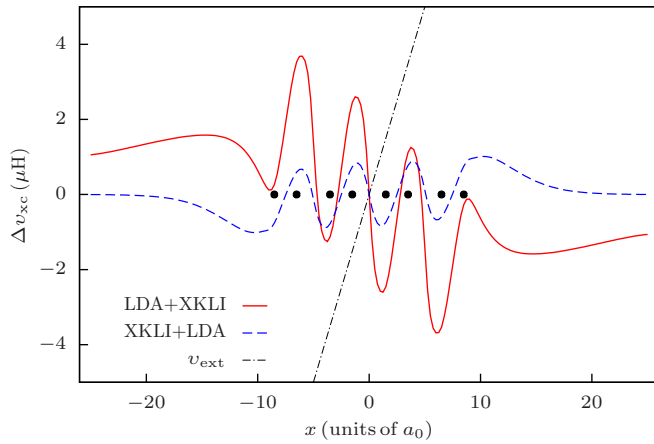


FIG. 5. Linear-response results for $\Delta v_{xc}(\mathbf{r})$ calculated from Eq. (64) using combinations of two different xc approximations in the GS calculation and the subsequent construction of $v_{xc}^{(+)}(\mathbf{r})$.

identical to the XKLI and LDA potentials, respectively. This proves that the functional used to construct $v_{xc}^{(+)}(\mathbf{r})$ is almost exclusively responsible for its resulting spatial structure, while the functional used in the GS calculation has only very little influence on these results.

APPENDIX D: REFERENCE SPECTRA FOR Na₅

The purpose of the calculations presented in Sec. VIC is only to show that, with our method, stable and robust XKLI calculations can be done even for the extreme case of Na₅, in spite of this system's known propagation instabilities. However, it is also useful to verify that the resulting XKLI spectrum is physically reasonable. To that purpose, we compare in this section the XKLI spectrum to other calculations and to the experiment [108].

Our calculated spectra using the exchange-only local-density approximation (XLDA), a combination of the XKLI GS with the XLDA response potential (XKLI+XLDA), the Hartree-Fock scheme (HF), and the hybrid functional PBE0 [109,110] in the generalized Kohn-Sham scheme (GKS-PBE0) are depicted in Fig. 6 [111]. The experimental spectrum is rather broad and featureless and only allows to identify the main absorption peak at approximately 2.05 eV. This is well reproduced by the XKLI (approximately 2.11 eV), better than, e.g., with the XLDA.

Comparing the different calculated spectra shows that the XKLI spectrum agrees at least qualitatively rather well with the other results. Somewhat surprisingly, the HF, which is conceptually close to the XKLI in that it is based on the same orbital-dependent energy expression, yields a spectrum that

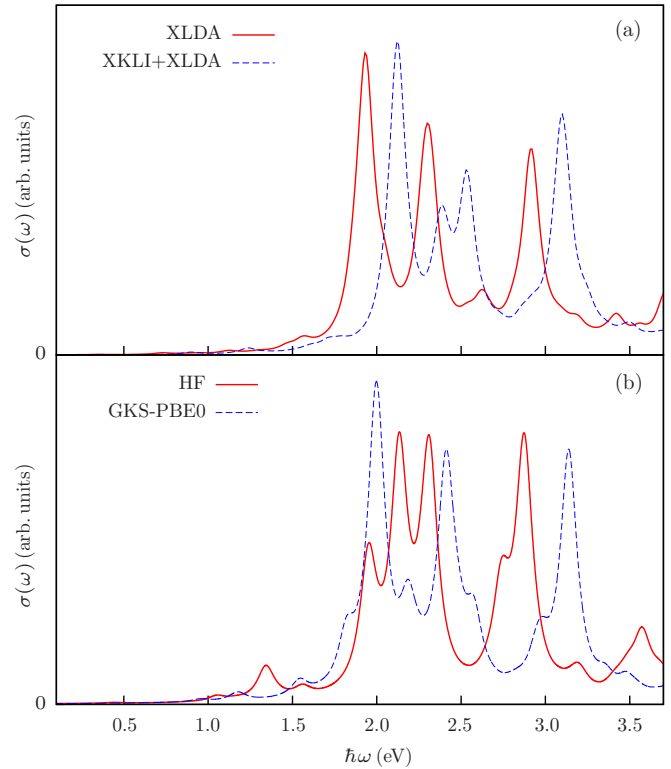


FIG. 6. Photoabsorption spectra of Na₅ calculated with different approximations: (a) exchange-only local density approximation (XLDA) and a combination of the XKLI GS with the XLDA response potential (XKLI+XLDA) and (b) Hartree-Fock (HF) and the hybrid functional PBE0 in the generalized Kohn-Sham scheme (GKS-PBE0).

differs more from the XKLI than any of the other spectra. We carefully tested that this is not merely due to the difference between basis sets and real-space grid-based numerics. All spectra except the HF show three rather-well-defined peaks at about 2.0, 2.5, and 3.0 eV and some smaller peaks in between, with the XLDA spectrum slightly redshifted by approximately 0.2 eV compared to XKLI, XKLI+XLDA, and PBE0. The HF spectrum also has the peak at approximately 3.0 eV but a somewhat different structure between 2.0 and 2.5 eV.

Since the Na₅ spectrum does not contain excitations of, e.g., charge transfer character, it is not surprising that the XKLI and XKLI+XLDA are quite similar. Slightly more unexpected is the good agreement between XKLI and PBE0, as the latter contains only 25% exact exchange and as the generalized Kohn-Sham treatment of this exact exchange is similar to the HF.

- [1] T. Grabo, T. Kreibich, S. Kurth, and E. K. U. Gross, in *Strong Coulomb Correlation in Electronic Structure: Beyond the Local Density Approximation*, edited by V. Anisimov (Gordon & Breach, Tokyo, 2000), pp. 203–311.
- [2] M. A. L. Marques and E. K. U. Gross, *Annu. Rev. Phys. Chem.* **55**, 427 (2004).

- [3] A. D. Becke, *J. Chem. Phys.* **98**, 5648 (1993).
- [4] R. E. Stratmann, G. E. Scuseria, and M. J. Frisch, *J. Chem. Phys.* **109**, 8218 (1998).
- [5] F. Furche and R. Ahlrichs, *J. Chem. Phys.* **117**, 7433 (2002).
- [6] J. Jaramillo, G. E. Scuseria, and M. Ernzerhof, *J. Chem. Phys.* **118**, 1068 (2003).

- [7] A. V. Arbuznikov, M. Kaupp, and H. Bahmann, *J. Chem. Phys.* **124**, 204102 (2006).
- [8] J. P. Perdew, V. N. Staroverov, J. M. Tao, and G. E. Scuseria, *Phys. Rev. A* **78**, 052513 (2008).
- [9] T. Schmidt, E. Kraisler, A. Makmal, L. Kronik, and S. Kümmel, *J. Chem. Phys.* **140**, 18A510 (2014).
- [10] T. M. Maier, H. Bahmann, A. V. Arbuznikov, and M. Kaupp, *J. Chem. Phys.* **144**, 074106 (2016).
- [11] H. Iikura, T. Tsuneda, T. Yanai, and K. Hirao, *J. Chem. Phys.* **115**, 3540 (2001).
- [12] M. Henderson, B. G. Janesko, and G. E. Scuseria, *J. Chem. Phys.* **128**, 194105 (2008).
- [13] J. Heyd, G. E. Scuseria, and M. Ernzerhof, *J. Chem. Phys.* **118**, 8207 (2003).
- [14] T. Yanai, D. P. Tew, and N. C. Handy, *Chem. Phys. Lett.* **393**, 51 (2004).
- [15] J.-D. Chai and M. Head-Gordon, *J. Chem. Phys.* **128**, 084106 (2008).
- [16] M. A. Rohrdanz, K. M. Martins, and J. M. Herbert, *J. Chem. Phys.* **130**, 054112 (2009).
- [17] L. Kronik, T. Stein, S. Refaely-Abramson, and R. Baer, *J. Chem. Theory Comput.* **8**, 1515 (2012).
- [18] M. A. L. Marques, A. Castro, and A. Rubio, *J. Chem. Phys.* **115**, 3006 (2001).
- [19] C. Legrand, E. Suraud, and P.-G. Reinhard, *J. Phys. B* **35**, 1115 (2002).
- [20] P. M. Dinh, J. Messud, P. G. Reinhard, and E. Suraud, *J. Phys.: Conf. Ser.* **248**, 012024 (2010).
- [21] D. Hofmann, T. Körzdörfer, and S. Kümmel, *Phys. Rev. Lett.* **108**, 146401 (2012).
- [22] X.-M. Tong and S.-I. Chu, *Int. J. Quantum Chem.* **69**, 293 (1998).
- [23] C. A. Ullrich, P.-G. Reinhard, and E. Suraud, *Phys. Rev. A* **62**, 053202 (2000).
- [24] S.-I. Chu, *J. Chem. Phys.* **123**, 062207 (2005).
- [25] M. Dauth and S. Kümmel, *Phys. Rev. A* **93**, 022502 (2016).
- [26] F. Krečinić, P. Wopperer, B. Frusteri, F. Brauße, J.-G. Brisset, U. De Giovannini, A. Rubio, A. Rouzée, and M. J. J. Vrakking, *Phys. Rev. A* **98**, 041401 (2018).
- [27] O. A. Vydrov, G. E. Scuseria, and J. P. Perdew, *J. Chem. Phys.* **126**, 154109 (2007).
- [28] D. Hofmann and S. Kümmel, *Phys. Rev. B* **86**, 201109(R) (2012).
- [29] D. Hofmann and S. Kümmel, *J. Chem. Phys.* **137**, 064117 (2012).
- [30] R. Baer and L. Kronik, *Eur. Phys. J. B* **91**, 170 (2018).
- [31] F. Della Sala and A. Görling, *Int. J. Quantum Chem.* **91**, 131 (2003).
- [32] N. T. Maitra, T. N. Todorov, C. Woodward, and K. Burke, *Phys. Rev. A* **81**, 042525 (2010).
- [33] M. Thiele and S. Kümmel, *Phys. Rev. Lett.* **112**, 083001 (2014).
- [34] Y. Suzuki, L. Lacombe, K. Watanabe, and N. T. Maitra, *Phys. Rev. Lett.* **119**, 263401 (2017).
- [35] C. A. Ullrich, U. J. Gossmann, and E. K. U. Gross, *Phys. Rev. Lett.* **74**, 872 (1995).
- [36] Y.-H. Kim and A. Görling, *Phys. Rev. Lett.* **89**, 096402 (2002).
- [37] S. Hirata, S. Ivanov, I. Grabowski, and R. J. Bartlett, *J. Chem. Phys.* **116**, 6468 (2002).
- [38] S. Hirata, S. Ivanov, R. J. Bartlett, and I. Grabowski, *Phys. Rev. A* **71**, 032507 (2005).
- [39] S. Hirata, *J. Chem. Phys.* **123**, 026101 (2005).
- [40] Y. Shigeta, K. Hirao, and S. Hirata, *Phys. Rev. A* **73**, 010502 (2006).
- [41] F. Bruneval, F. Sottile, V. Olevano, and L. Reining, *J. Chem. Phys.* **124**, 144113 (2006).
- [42] M. Hellgren and U. von Barth, *Phys. Rev. B* **78**, 115107 (2008).
- [43] M. Hellgren and U. von Barth, *J. Chem. Phys.* **131**, 044110 (2009).
- [44] A. Heßelmann, A. Ipatov, and A. Görling, *Phys. Rev. A* **80**, 012507 (2009).
- [45] A. Ipatov, A. Heßelmann, and A. Görling, *Int. J. Quantum Chem.* **110**, 2202 (2010).
- [46] A. Heßelmann and A. Görling, *J. Chem. Phys.* **134**, 034120 (2011).
- [47] K. Yabana and G. F. Bertsch, *Phys. Rev. B* **54**, 4484 (1996).
- [48] M. Mundt and S. Kümmel, *Phys. Rev. A* **74**, 022511 (2006).
- [49] H. O. Wijewardane and C. A. Ullrich, *Phys. Rev. Lett.* **95**, 086401 (2005).
- [50] I. Schelter, Numerische Lösung des Optimized Effective Potential, M.Sc. thesis, University of Bayreuth, 2013.
- [51] S.-L. Liao, T.-S. Ho, H. Rabitz, and S.-I. Chu, *Phys. Rev. Lett.* **118**, 243001 (2017).
- [52] J. B. Krieger, Y. Li, and G. J. Iafrate, *Phys. Rev. A* **46**, 5453 (1992).
- [53] O. V. Gritsenko and E. J. Baerends, *Phys. Rev. A* **64**, 042506 (2001).
- [54] F. Della Sala and A. Görling, *J. Chem. Phys.* **115**, 5718 (2001).
- [55] M. Mundt, S. Kümmel, R. van Leeuwen, and P. G. Reinhard, *Phys. Rev. A* **75**, 050501 (2007).
- [56] J. Messud, P. M. Dinh, P.-G. Reinhard, and E. Suraud, *Phys. Rev. A* **80**, 044503 (2009).
- [57] X. Andrade, S. Botti, M. A. L. Marques, and A. Rubio, *J. Chem. Phys.* **126**, 184106 (2007).
- [58] F. Hofmann, I. Schelter, and S. Kümmel, *J. Chem. Phys.* **149**, 024105 (2018).
- [59] S. Baroni, S. De Gironcoli, A. Dal Corso, and P. Giannozzi, *Rev. Mod. Phys.* **73**, 515 (2001).
- [60] S. Y. Savrasov, *Phys. Rev. Lett.* **81**, 2570 (1998).
- [61] J.-I. Iwata, K. Yabana, and G. F. Bertsch, *J. Chem. Phys.* **115**, 8773 (2001).
- [62] M. J. T. Oliveira, A. Castro, M. A. L. Marques, and A. Rubio, *J. Nanosci. Nanotechnol.* **8**, 3392 (2008).
- [63] H. Hübener and F. Giustino, *Phys. Rev. B* **89**, 085129 (2014).
- [64] H. Hübener and F. Giustino, *J. Chem. Phys.* **141**, 044117 (2014).
- [65] K. Cao, H. Lambert, P. G. Radaelli, and F. Giustino, *Phys. Rev. B* **97**, 024420 (2018).
- [66] *Fundamentals Of Time-Dependent Density Functional Theory*, edited by M. A. L. Marques, N. T. Maitra, F. M. S. Nogueira, E. K. U. Gross, and A. Rubio, Lecture Notes in Physics Vol. 837 (Springer, Heidelberg, 2012).
- [67] R. van Leeuwen, *Int. J. Mod. Phys. B* **15**, 1969 (2001).
- [68] E. Runge and E. K. U. Gross, *Phys. Rev. Lett.* **52**, 997 (1984).
- [69] M. E. Casida, *J. Mol. Struct. THEOCHEM* **914**, 3 (2009).
- [70] J. Chen, J. B. Krieger, Y. Li, and G. J. Iafrate, *Phys. Rev. A* **54**, 3939 (1996).

- [71] T. Körzdörfer, M. Mundt, and S. Kümmel, *Phys. Rev. Lett.* **100**, 133004 (2008).
- [72] J. C. Slater, *Phys. Rev.* **81**, 385 (1951).
- [73] R. T. Sharp and G. K. Horton, *Phys. Rev.* **90**, 317 (1953).
- [74] M. Grüning, O. V. Gritsenko, and E. J. Baerends, *J. Chem. Phys.* **116**, 6435 (2002).
- [75] V. U. Nazarov, *Phys. Rev. B* **87**, 165125 (2013).
- [76] D. G. Anderson, *J. ACM* **12**, 547 (1965).
- [77] J. P. Perdew and A. Zunger, *Phys. Rev. B* **23**, 5048 (1981).
- [78] M. Mundt, S. Kümmel, B. Huber, and M. Moseler, *Phys. Rev. B* **73**, 205407 (2006).
- [79] M. Mundt and S. Kümmel, *Phys. Rev. B* **76**, 035413 (2007).
- [80] L. Kronik, A. Makmal, M. L. Tiago, M. M. G. Alemany, M. Jain, X. Huang, Y. Saad, and J. R. Chelikowsky, *Phys. Status Solidi B* **243**, 1063 (2006).
- [81] N. Troullier and J. L. Martins, *Phys. Rev. B* **43**, 1993 (1991).
- [82] L. Kleinman and D. M. Bylander, *Phys. Rev. Lett.* **48**, 1425 (1982).
- [83] D. Hofmann, Charge and excitation-energy transfer in time-dependent density functional theory, Ph.D. thesis, University of Bayreuth, 2012.
- [84] B. Champagne, D. H. Mosley, M. Vračko, and J.-M. André, *Phys. Rev. A* **52**, 178 (1995).
- [85] S. J. A. van Gisbergen, P. R. T. Schipper, O. V. Gritsenko, E. J. Baerends, J. G. Snijders, B. Champagne, and B. Kirtman, *Phys. Rev. Lett.* **83**, 694 (1999).
- [86] M. van Faassen, P. L. de Boeij, R. van Leeuwen, J. A. Berger, and J. G. Snijders, *Phys. Rev. Lett.* **88**, 186401 (2002).
- [87] M. van Faassen and N. Maitra, *J. Chem. Phys.* **126**, 191106 (2007).
- [88] S. Kümmel, L. Kronik, and J. P. Perdew, *Phys. Rev. Lett.* **93**, 213002 (2004).
- [89] P. Umari, A. J. Williamson, G. Galli, and N. Marzari, *Phys. Rev. Lett.* **95**, 207602 (2005).
- [90] A. Ruzsinszky, J. P. Perdew, G. I. Csonka, G. E. Scuseria, and O. A. Vydrov, *Phys. Rev. A* **77**, 060502(R) (2008).
- [91] A. Ruzsinszky, J. P. Perdew, and G. I. Csonka, *Phys. Rev. A* **78**, 022513 (2008).
- [92] C. D. Pemmaraju, S. Sanvito, and K. Burke, *Phys. Rev. B* **77**, 121204(R) (2008).
- [93] B. Champagne and B. Kirtman, *Int. J. Quantum Chem.* **109**, 3103 (2009).
- [94] T. Körzdörfer and S. Kümmel, in *Theoretical and Computational Developments in Modern Density Functional Theory*, edited by A. K. Roy (Nova Science, New York, 2012), pp. 211–222.
- [95] The eight H atoms are aligned on the x axis with alternating distances of $2a_0$ and $3a_0$. We use an ellipsoidal simulation sphere with a half axis of $25a_0$ in the x direction and $15a_0$ in the y and z directions. The spacing of our cubic grid is $0.25a_0$ and the cutoff radius of the LDA pseudopotential we use to describe the H atoms is $1.39a_0$.
- [96] I. Schelter and S. Kümmel, *J. Chem. Theory Comput.* **14**, 1910 (2018).
- [97] We use a simulation sphere radius of $16a_0$, a grid spacing of $0.5a_0$, a Si-H bond length of 1.474 \AA , and LDA pseudopotentials with cutoff radii of $1.79a_0$ for Si and $1.39a_0$ for H. In the linear-response calculations we use $\hbar\eta = 25 \text{ meV}$ (corresponding to Lorentzian linewidths of $2\hbar\eta = 0.05 \text{ eV}$) and a frequency step size of $\hbar\Delta\omega = 15 \text{ meV}$. The real-time propagations are done with a boost strength of $E_{\text{boost}} = 1 \mu\text{Ry}$, a time step of 1 as , and a fourth-order Taylor propagator. To facilitate the comparison to the Sternheimer spectra, the real-time dipole moment is multiplied with an exponential decay factor prior to the Fourier transform, leading to Lorentzian line shapes.
- [98] A. Karolewski, R. Armiento, and S. Kümmel, *Phys. Rev. A* **88**, 052519 (2013).
- [99] M. Levy and J. P. Perdew, *Phys. Rev. A* **32**, 2010 (1985).
- [100] G. Vignale, *Phys. Rev. Lett.* **74**, 3233 (1995).
- [101] J. Messud, P. M. Dinh, P. G. Reinhard, and E. Suraud, *Ann. Phys. (Berlin)* **523**, 270 (2011).
- [102] R. Ahlrichs, M. Bär, M. Häser, H. Horn, and C. Kölmel, *Chem. Phys. Lett.* **162**, 165 (1989).
- [103] P. J. Stephens, F. J. Devlin, C. F. Chabalowski, and M. J. Frisch, *J. Phys. Chem.* **98**, 11623 (1994).
- [104] F. Weigend and R. Ahlrichs, *Phys. Chem. Chem. Phys.* **7**, 3297 (2005).
- [105] We use a spherical grid with a radius of $21a_0$ and spacing of $0.7a_0$, a LDA pseudopotential with a cutoff radius of $3.09a_0$, $\hbar\eta = 60 \text{ meV}$, and a step size of $\hbar\Delta\omega = 10 \text{ meV}$. The Na atoms are located in the xz plane at $(x, z) = (\pm 3.329a_0, 3.393a_0)$, $(\pm 6.432a_0, -2.219a_0)$, and $(0.000a_0, -2.348a_0)$.
- [106] I. A. Solov'yov, A. V. Solov'yov, and W. Greiner, *Phys. Rev. A* **65**, 053203 (2002).
- [107] S. Kümmel and J. P. Perdew, *Phys. Rev. B* **68**, 035103 (2003).
- [108] C. R. C. Wang, S. Pollack, T. A. Dahlseid, G. M. Koretsky, and M. M. Kappes, *J. Chem. Phys.* **96**, 7931 (1992).
- [109] J. P. Perdew, M. Ernzerhof, and K. Burke, *J. Chem. Phys.* **105**, 9982 (1996).
- [110] J. P. Perdew, K. Burke, and M. Ernzerhof, *Phys. Rev. Lett.* **77**, 3865 (1996).
- [111] The XLDA and XKLI+XLDA calculations are done with the same grid, pseudopotential, η value, and frequency step size as in Sec. VI C. For the HF and GKS-PBE0 calculations, we use TURBOMOLE and the def2-QZVP [104] basis set. To ease comparisons, the “stick spectra” obtained with TURBOMOLE were folded with Lorentzians with a width of 0.12 eV .